https://doi.org/10.5194/egusphere-2026-457
Preprint. Discussion started: 5 March 2026

Country-wide rainfall estimates from a commercial microwave link network in Belgium

Kwinten Van Weverberg[1,2], Nina Neutens[2], Simon De Corte[2], Armani Passtoors[2], Stephan Calderan[3], Nicolas Ghilain[1,4], Ricardo Reinoso-Rondinel[1,5], Maarten Reyniers[1], Aart Overeem[6], Hans Van de Vyver[1], Bert Van Schaeybroeck[1,2], Bart De Wit[2], and Remko Uijlenhoet[7]

[1]Royal Meteorological Institute of Belgium, Belgium
[2]Department of Geography, Ghent University, Belgium
[3]Telenet Group N.V., Belgium
[4]Department of Geography, Liège University, Belgium
[5]Department of Civil Engineering, KULeuven, Belgium
[6]R&D Observations and Data Technology, Royal Netherlands Meteorological Institute, The Netherlands
[7]Department of Water Management, Delft University of Technology, The Netherlands

Correspondence: Kwinten Van Weverberg (kwinten.vanweverberg@ugent.be)

Abstract. Accurate quantitative precipitation estimation (QPE) at high spatiotemporal resolution remains challenging despite advances in observational technology. This study presents the first comprehensive evaluation of rainfall retrievals from a commercial microwave link (CML) network in Belgium, examining whether CML-derived rainfall can complement existing dense rain gauge and weather radar networks. We analyze four intense summer rainfall events in 2023 using over 2800 microwave (sub)links operating across frequencies from 10 to 85 GHz. Through systematic sensitivity experiments, we assess the impact of optimizing the processing procedures. Our results demonstrate that careful processing of CML data is essential: a novel outlier filtering algorithm, radar-based wet-dry classification, rainfall-intensity-dependent wet-antenna correction, and fitting local drop size distributions from three disdrometers substantially improve rainfall retrievals. The optimized CML-derived rainfall estimates match or exceed the performance of a state-of-the-art radar-gauge merged product compared to a dense rain-gauge network, particularly over urban areas with dense high-frequency link coverage, like the Brussels-Capital Region. These findings provide strong evidence that integration of CML information into multi-source precipitation products could yield substantial improvements in high-resolution QPE, particularly for urban hydrological applications and extreme-event monitoring.

1 Introduction

Accurate quantitative precipitation estimation (QPE) at high spatiotemporal resolution is essential for catchment- and city-scale hydrological applications, ranging from infrastructure planning to pluvial and fluvial flood warning systems and insurance-claim assessments (Hailegeorgis and Alfredsen, 2017; Johnson et al., 2020; Sokol et al., 2021). However, QPE remains challenging due to the large spatiotemporal variability of precipitation and the variability in precipitation microphysical properties such as the drop size distribution, which affect remote sensing retrievals (Uijlenhoet, 2001; Chen et al., 2023). Consequently,

https://doi.org/10.5194/egusphere-2026-457
Preprint. Discussion started: 5 March 2026

even dense rain gauge networks under-sample rainfall (Lengfeld et al., 2020), while remote sensing techniques such as weather radar require retrieval relations with parameters depending on local raindrop size distributions. In addition, error sources such as beam blocking, signal attenuation, and non-meteorological echoes further complicate the retrieval of rainfall estimates using radar. Considerable effort has been dedicated to combining the strengths of each measurement technique through advanced merging algorithms (Schuurmans et al., 2007; Goudenhoofdt and Delobbe, 2009; Moraux et al., 2021).

In recent decades, a novel opportunistic source of rainfall estimates has emerged through the exploitation of signal attenuation in commercial telecommunication networks (commercial microwave links, CMLs; Messer et al. (2006); Leijnse et al. (2007); Chwala and Kunstmann (2019); Uijlenhoet et al. (2018)). The presence of very dense networks has enabled the retrieval of accurate, high-resolution rainfall estimates in numerous countries. However, as with radar and rain gauges, several limitations and error sources affect CML-derived rainfall. While standard procedures have been developed to derive rainfall from CML signals (Overeem et al., 2016a), they are usually not validated when applied over new regions or settings, mostly due to lack of observational datasets. For instance, while the retrieval of rainfall information from signal attenuation is, in principle, less dependent on microphysical properties for intermediate microwave frequencies around 20–30 GHz compared to weather radar (3–10 GHz), this dependency becomes more pronounced at lower and higher microwave frequencies. Additionally, wet antennas contribute to the overall signal attenuation, which needs to be accounted for. Other error sources include inaccurate hardware calibration of antennas, wind effects on telecommunication towers, limited power resolution of received signal levels, unresolved rainfall variability along the link between transmitter and receiver, and attenuation from obstacles, water vapor, and trace gases (Chwala and Kunstmann (2019)). Lastly, it is not always straightforward to map and spatially interpolate the often inhomogeneous network. Conversely, compared to radar, CML-derived rainfall offers the advantage of enabling rainfall estimation typically closer to the surface, thereby avoiding beam overshooting and evaporation of detected rainfall below the beam. Furthermore, CML-derived rainfall is less affected by beam broadening and non-uniform beam-filling, given the typically limited distances (several 100 m to a few km) between the antennas (Berne and Uijlenhoet, 2007), although in the tropics one often finds very long (10 - 25 km) low-frequency (< 10 GHz) links, with more significant non-uniform beam filling effects as consequence.

While dense rain gauge and radar networks exist throughout most of Western Europe, North America and East Asia, the question remains whether the additional source of rainfall information from CMLs can meaningfully contribute to multimodal quantitative rainfall estimation. This paper provides the first evaluation of rainfall obtained from a CML network in Belgium, which exhibits substantial spatial overlap with a dense operational rain gauge and radar network. The objective of this research is to determine whether this CML-dataset provides added value compared to the existing combination of radar and rain gauges for several cases of intense summertime precipitation. In addition, we assess whether the quality of rainfall retrievals can be optimized by introducing a novel outlier filtering algorithm, implementing various techniques for wet-antenna correction and wet-dry classification, and re-fitting the attenuation-rainfall relation based on locally observed drop size distributions from three disdrometers within the domain. This relationship is typically obtained from globally fitted rainfall observations published by the International Telecommunication Union (ITU, 2005).

https://doi.org/10.5194/egusphere-2026-457
Preprint. Discussion started: 5 March 2026

The remainder of this paper is organized as follows. Section 2 describes all datasets, including CML, rain gauge, radar, and disdrometer data. Section 3 outlines the sensitivity experiments and optimization techniques. Section 4 presents the key results, which are discussed in Section 5. Conclusions are provided in Section 6.

2 Case Description and Data

2.1 Case Description

This paper focuses on four extreme rainfall events that occurred in Belgium in June and July 2023, for which the Royal Meteorological Institute of Belgium (RMI) issued at least a yellow warning for rain ('being alert' for rain intensities of at least 20 mm in one hour or 25 mm in 24 hours; RMI).

On 22 June 2023 (Case 1), warm, moist air moved toward southern Belgium from the Mediterranean, driven by a small deepening depression moving northward. This resulted in widespread intense rainfall and embedded thunderstorms, particularly over the southern hills of Belgium. The RMI issued a red warning (i.e. rainfall exceeding 50 mm in one hour, 60 mm in 6 hours or 100 mm in 24 hours; RMI) for the province of Namur for rainfall, and an orange warning (i.e. rainfall exceeding 30 mm in one hour, 40 mm in 6 hours or 50 mm in 24 hours; RMI) for all other southern provinces. Several stations recorded such rainfall amounts with the 99th percentile accumulations exceeding 55 mm over 24 hours (Table 1).

Table 1. General statistics of case-accumulated precipitation across all 204 rain gauges shown in Figure 1 and for all cases. Shown are the case Duration, Mean Accumulations (Acc), 99th Percentile of the case-accumulations (P99) and the Standard Deviation of the accumulations (Std) across all stations. In addition, the mean of each metric across the four cases is shown.

Case	Duration	Acc (mm)	P99 (mm)	Std (mm)
Case 1	22 June 2023 (24 hours)	21.5	55.2	14.8
Case 2	8-9 July 2023 (48 hours)	3.0	15.7	3.4
Case 3	23-24 July 2023 (48 hours)	20.1	47.6	14.0
Case 4	28-29 July 2023 (48 hours)	10.5	46.3	10.3

On 8 and 9 July 2023 (Case 2), local thunderstorms developed over Belgium, following a brief hot spell, ahead of a cold front advancing from the west, associated with a deep depression west of Ireland. The RMI issued an orange warning for eastern Belgium for thunderstorms, bringing rainfall accumulations exceeding 20-40 mm h^{-1} and a risk of large hail. A substantial mesoscale convective system developed during the afternoon, primarily affecting northeastern Belgium.

During the night of 23 to 24 July 2023 (Case 3), an intense wave developed along a cold front crossing Belgium, associated with a depression tracking from Scotland to Denmark. This produced several waves of very intense rainfall, predominantly over central Belgium, followed by widespread showers. The RMI issued a yellow warning for rainfall amounts up to 50 mm within 24 hours.

https://doi.org/10.5194/egusphere-2026-457
Preprint. Discussion started: 5 March 2026

On 28 and 29 July (Case 4), an intense frontal system was followed by widespread showers over an extended period, primarily affecting southern Belgium. The RMI issued a yellow warning for rainfall amounts exceeding 50 mm within 48 hours.

2.2 Commercial Microwave Link Data

Network performance data from the mobile network operator Telenet N.V. were obtained for the four cases presented. This dataset comprises over 1600 CMLs (and about 2800 sublinks) across Belgium, with particularly high density near the cities of Liège, Brussels, and Charleroi. Figure 1a shows the distribution of CMLs throughout the country. Relatively fewer links are available in northern provinces, where fiber-optic cable has become the dominant communication medium between mobile network towers. The network consists of microwave frequencies ranging from 7 to 85 GHz, with most links operating between 20 and 30 GHz and spanning lengths of a few kilometers (Figure 2). Short, high-frequency links are predominantly located near major cities in southern and central Belgium.

The network management system records the minimum and maximum transmitted and received signal power at 15-minute intervals for all links in the network with a precision of 1 dB. For most links (about 65 %), transmitted power is adjusted in the event of power loss due to rainfall (so-called automatic transmit-power control - ATPC). To calculate the average power loss over a 15-minute time window (caused by attenuation due to rain, atmospheric gasses, and free-space losses; TRSL), we subtract the average of the minimum and maximum received signal level (RSL) from the average of the minimum and maximum transmitted signal level (TSL). In addition to the received and transmitted power levels for each (sub)link, the performance system records the background block error, severely errored seconds, errored seconds, and unavailable seconds, which we use as a first quality flag. Any 15-minute periods for a particular link with non-zero values for these error estimates were omitted from further data analysis (approximately 1–2% of the complete dataset).

Note that the reported power loss, TRSL (dB), from the network management system, is not only caused by rainfall. Indeed, even in dry conditions, free space losses, trace gases, aerosols and water vapor contribute to the attenuation (A_{dry}, dB). In addition, water droplets on the antennas during rain events also cause attenuation, not-directly caused by falling raindrops (wet-antenna attenuation, A_{waa}, dB). This implies that the specific, i.e. path-averaged, attenuation (dB km^{-1}) to be used in rainfall retrievals, further referred to as γ), along the CML path is:

$$\gamma = TRSL/L - A_{waa}/L - A_{dry}/L, \tag{1}$$

where A_{waa} (dB) is the wet antenna attenuation, A_{dry} (dB) is the baseline dry attenuation, and L is the distance (km) between the antennas for the CML of interest.

Rainfall rates from the power loss can then be obtained by inverting the specific attenuation (γ)-rain rate (R) relation:

$$\gamma = a \cdot R^b, \tag{2}$$

https://doi.org/10.5194/egusphere-2026-457
Preprint. Discussion started: 5 March 2026

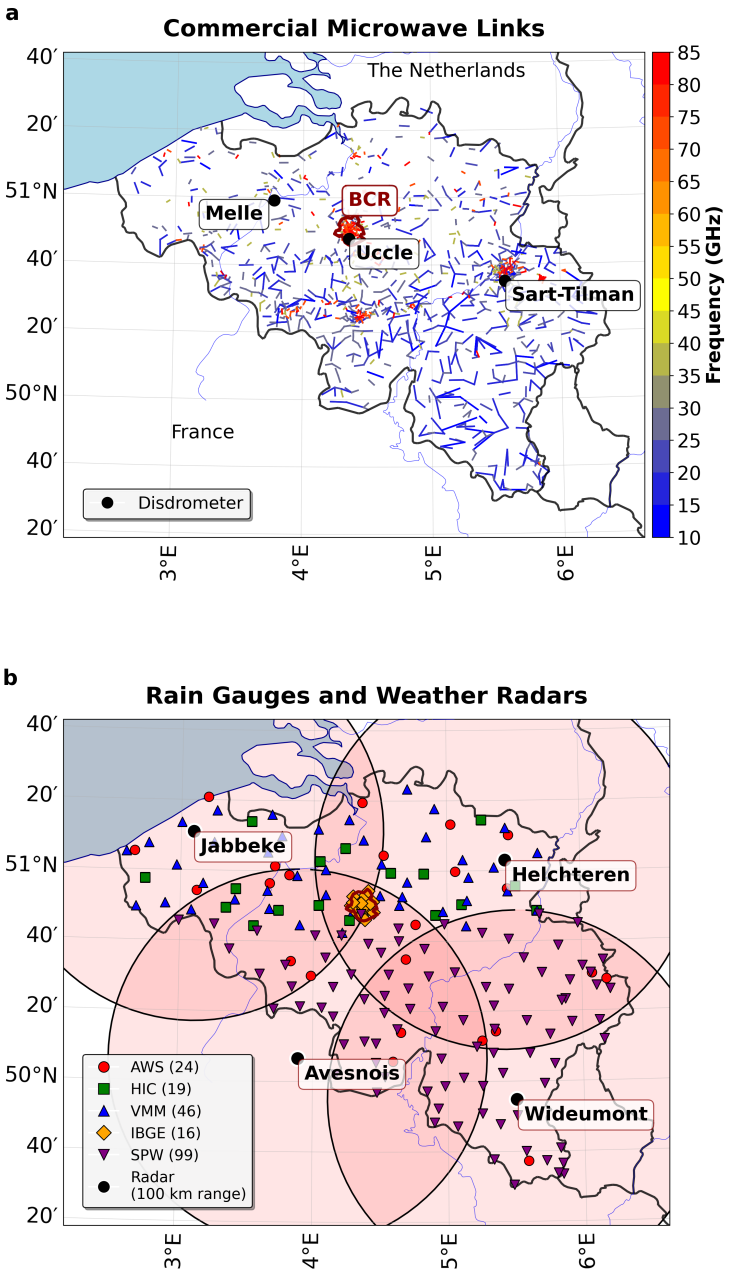

Figure 1. Spatial distribution of (a) CML network and disdrometers and (b) rain-gauge and weather radar networks in Belgium as used in this study. The colors of the CMLs reflect their operating frequency. The rain-gauge networks have different symbols as outlined in the legend. A 100 km radius around each radar site is shown by the black circles. The red outline of the Brussels-Capital Region (BCR) is also shown, for reference (see Section 4.5).

https://doi.org/10.5194/egusphere-2026-457
Preprint. Discussion started: 5 March 2026

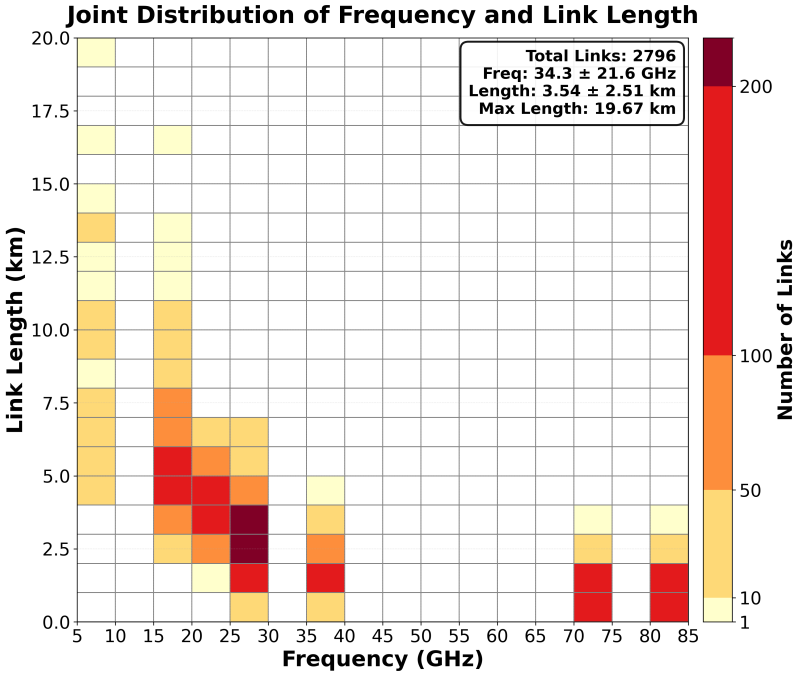

Figure 2. Joint distribution of the frequencies (X-axis) and lengths (Y-axis) of the CML network in Belgium. Numbers in the box denote the average and standard deviation of CML frequency and length, as well as the total number of sublinks and the maximum CML length.

where γ is the specific attenuation (dB km^{-1}), R is the rain rate (mm h^{-1}), and a and b are power-law fitting parameters.

We use the pycomlink open-source software (Chwala et al., 2025) for the CML processing and disaggregation of the reported attenuation in its constituents as in Equation 1, and to obtain rainfall estimates from γ employing the standard International Telecommunication Union values for a and b (ITU, 2005) as in Equation 2. However, we also re-fitted this relation specifically for conditions typical of summer in Belgium using disdrometer observations, as outlined in Section 3.4. Further information on outlier filtering methods, the choice of wet-dry classification, employed to assess the baseline attenuation and to prevent non-zero rainfall estimation during dry weather, and wet-antenna attenuation correction is provided in Section 3. Note that for all rainfall retrievals from the CML attenuation, we assume the rainfall to be valid for the midpoint of the respective link. We treat all sublinks with valid data as independent data points.

2.3 Rain Gauge Data

Several agencies in Belgium operate sub-hourly rain gauge networks. These include automatic weather stations (AWS) operated by the RMI, the Flemish Environment Agency (Vlaamse Milieumaatschappij; VMM), the Hydrological Information Centre (HIC) as part of Flanders Hydraulics (Hydrologisch Informatie Centrum; HIC), the Walloon Hydrological Management Agency (Gestion Hydrologique) from the Service Public de Wallonie (SPW) Mobilité et Infrastructures, and the Brussels Environment Management Institute (Institut Bruxellois pour la Gestion de l'Environnement; IBGE). All these networks operate at 5-minute

https://doi.org/10.5194/egusphere-2026-457
Preprint. Discussion started: 5 March 2026

temporal resolution. Locations of all rain gauges are shown in Figure 1b. In total, 204 sub-hourly rain gauge stations were used in the analysis. The 5-minute rain gauge data were aggregated to a 15-min frequency for direct comparison against the radar and CML rainfall estimates. An interpolated product solely based on all rain gauges was created, using the ordinary kriging procedures from pycomlink. This is the same procedure as was applied to interpolate the CML-derived rainfall, using a daily-varying climatological spherical variogram obtained from 30 years of rain gauge data in The Netherlands, as described in Overeem et al. (2016a) and van de Beek et al. (2012).

2.4 Radar Data

A dense C-band dual-polarization weather radar network covers Belgium (Figure 1b), including two radars operated by the RMI near the coast at Jabbeke (51.18°N, 3.10°E) and in southern Belgium near Wideumont (49.91°N, 5.50°E; Berne et al. (2005)). In addition, a radar operated by the VMM covers most of northeastern Belgium (Helchteren, 51.05°N, 5.44°E), and a radar near l'Avesnois in France, operated by Météo France, provides additional coverage in the southwestern part of the country (50.11°N, 3.89°E). The location of the radars and a 100 km radius surrounding them is provided in Figure 1b.

We employ an operational merged radar-rain gauge product that incorporates all four operational radars and subhourly rain gauges described in the previous section, apart from the IBGE network. This product is developed by the RMI and adjusts the radar rainfall retrievals according to the technique described in Journée et al. (2023). This product, the so-called RAD-QPE product, is an operational rainfall estimate produced at 5-minute, 1-hour, and 1-day temporal resolution. The merging is performed using a mean-field bias adjustment. We refer to Journée et al. (2023) for further details on the rainfall processing of the radar and the specifics of the rain gauge-radar merging. The product used in this study is the 5-minute accumulation product, which was aggregated to 15-minute frequency to maintain consistency with the sub-hourly resolution of the other rainfall products employed (aggregating the three 5-minute values, without taking into account advection over a 5-minute interval).

2.5 Disdrometer Data

Three disdrometers have been continuously recording rain rates and raindrop size distributions over recent years in Belgium, which are used in this study to re-fit the $\gamma - \mathrm{R}$ relation for conditions typical of Belgium. The first disdrometer is operated by the University of Ghent and is located in Melle (50.99°N, 3.77°E). This is an OTT Hydromet Parsivel^2 laser disdrometer operating at 1-minute temporal frequency, recording raindrops using 32 size bins $\times$ 32 velocity bins. The disdrometer has been operational since May 2024, so no temporal overlap exists with the cases discussed in this study; nevertheless, we use the disdrometer data to derive typical relations between specific attenuation and rain rate for summers of 2024 and 2025, as outlined in the methods section. The second disdrometer is a Biral SWS-250 Present Weather Sensor at the RMI in Uccle (50.80°N, 4.36°E), operating at 5-minute temporal sampling frequency, and storing particle counts using a 21 size and 16 velocity bins matrix. Additionally, it provides hydrometer classification types (Bellot et al., 2011). This disdrometer has been operational since 2020. The third disdrometer is a Thies Clima Laser Precipitation Monitor, operational since 2005 at the University of Liège in Sart-Tilman (50.59°N, 5.57°E). It is one of the first-generation instruments of this type, using 20 size

https://doi.org/10.5194/egusphere-2026-457
Preprint. Discussion started: 5 March 2026

and 20 velocity classes to record the raindrop size distribution. This disdrometer has been used previously in several studies (e.g. Van Weverberg et al. (2024); Erpicum et al. (2012)). The location of each disdrometer is provided in Figure 1a.

3 Methods

In the following sections, several sensitivity experiments are described with the objective of improving the rainfall estimates derived from CMLs. An overview of all experiments is provided in Table 2.

3.1 Outlier Filtering

In addition to removing any instances with (severely) errored seconds, unavailable seconds, and background block error, further filtering was applied to detect microwave links that strongly deviate from their neighboring links. Indeed, beyond the reported quality flags, inaccuracies in link metadata, faulty hardware, or environmental conditions (e.g., obstruction by trees or swinging telecommunication towers under windy conditions) could lead to erroneous retrievals. Typical outlier filtering methods treat all links as independent, filtering out links that exhibit substantially different behavior compared to surrounding links. However, many links share antennas, primarily when they converge at so-called hubs. If issues occur at the location of a hub — for example, due to power instabilities or a swinging tower under windy conditions — a large number of links could be simultaneously affected by the same issue. Therefore, we developed an outlier-detection algorithm that compares each CML only with truly independent surrounding CMLs that share no antennas with one another or with the CML of interest. To implement this, we first performed a rainfall retrieval based on the unfiltered sublinks and computed, for each time instance, the accumulation over the preceding 24 hours. We then assessed the normalized rainfall deviation (Z-score) of each sublink from its neighboring links as follows:

$$Z = \frac{R_{sublink} - R_{neighbors}}{\sigma_{neighbors}}, \tag{3}$$

where $\mathrm{R_{sublink}}$ is the accumulation of CML rainfall over the preceding 24 hours. $\mathrm{R_{neighbors}}$ is the average accumulation over the past 24 hours, of all CMLs with their midpoints within a radius around the CML of interest. This radius is determined based on the time-varying spatial correlation estimated from 30-years of daily rain gauge data in The Netherlands (van de Beek et al., 2012). All CMLs within a circular distance of the CML in question, where the spatial correlation for that date exceeds 0.6, are considered neighboring CMLs, which are, by definition, expected to have similar rainfall amounts over a 24-hour period. $\sigma_{\mathrm{neighbors}}$ is the standard deviation of the 24-hour accumulation of neighboring CMLs. Note that only neighboring links that are truly independent (i.e., that share no towers) are considered. Of neighboring CMLs that do share a tower, only one sublink was randomly selected. Any link at a particular time instance for which Z exceeds a threshold of 2.5 is considered an outlier and is removed from the dataset. The value of the threshold spatial correlation and Z are optimal values for the four cases combined in this study (with small variability of these values between the cases), but could be adjusted should a longer CML dataset be available. This outlier filtering method can be applied in real-time if CML information of the past 24 hours is

https://doi.org/10.5194/egusphere-2026-457
Preprint. Discussion started: 5 March 2026

Table 2. Overview of all CML rainfall retrieval permutations. See text for details.

Long Name	Short Name	Outlier Filtering	Wet-Dry Classification	Wet-Antenna Correction	$\gamma - R$ relation
STANDARD DEVIATION-CONSTANT-ITU-UNFILTERED	SCI-U	No	Rolling Stdv Schleiss and Berne (2010)	Constant Overeem et al. (2016a)	ITU ITU (2005)
ROLLING-CONSTANT-ITU	SCI	Yes	Rolling Stdv Schleiss and Berne (2010)	Constant Overeem et al. (2016a)	ITU ITU (2005)
NEARLINK-CONSTANT-ITU	NCI	Yes	Nearby Links Overeem et al. (2016a)	Constant Overeem et al. (2016a)	ITU ITU (2005)
RADAR-CONSTANT-ITU	RCI	Yes	Radar	Constant Overeem et al. (2016a)	ITU ITU (2005)
RADAR-TIME-ITU	RTI	Yes	Radar	Time-dependent Schleiss et al. (2013)	ITU ITU (2005)
RADAR-INTENSITY-ITU	RII	Yes	Radar	Intensity-dependent Pastorek et al. (2022)	ITU ITU (2005)
RADAR-INTENSITY-DISDROMETER	RID	Yes	Radar	Intensity-dependent Pastorek et al. (2022)	Belgian disdrometers

https://doi.org/10.5194/egusphere-2026-457
Preprint. Discussion started: 5 March 2026

available. To understand the impact of outlier filtering, we compare the baseline, unfiltered rainfall estimates (SCI-U) with the outlier-filtered rainfall estimates (SCI). Note that SCI-U also includes the CMLs with errored seconds.

3.2 Wet-Dry Classification

An important aspect of rainfall detection using CMLs is the determination of the baseline (dry) attenuation, caused by free-space losses and constituents in the atmosphere like water vapor, aerosols and trace gases (Equation 1). Given that CMLs are often noisy, the classification of time series into wet and dry episodes is not straightforward. Over the past years, several methods have been proposed, including a rolling standard deviation method (Schleiss and Berne, 2010; Graf et al., 2024), methods using nearby links (Overeem et al., 2016a), and the use of auxiliary information such as radar (Overeem et al., 2011) or satellite data (van het Schip et al., 2017). To understand the importance of wet-dry classification, we apply several methods available in the pycomlink package, in addition to a method similar to Overeem et al. (2011), using the RAD-QPE product discussed in Section 2.4. The first iteration uses the rolling standard deviation method developed by Schleiss and Berne (2010). This method uses a moving time window and identifies dry periods as times when the TRSL variability within the time window is small, whereas wet periods are characterized by higher TRSL variability. We use a time window of 2 hours (i.e. 8 time steps) and the standard threshold for the standard deviation of 0.8 dB. The advantage of this method is that generally no calibration is needed and it can be applied to single-frequency and single-polarization CML signals, although it can be challenging to detect lighter rainfall (Schleiss and Berne, 2010). This rolling standard deviation method was also used in the experiments already described in the previous section (SCI-U and SCI).

A second method for discriminating between wet and dry periods follows the approach of Overeem et al. (2016a), using nearby links. The underlying assumption is that rain, and hence TRSL fluctuations, are spatially correlated. We apply this method using the default recommendation, requiring a minimum of 3 links within a 15 km radius and a threshold median (specific) attenuation of all links of -1.4 dB (-0.7 dB km^{-1}). Note that, since our CML data include only minimum and maximum transmitted and received power over a 15-minute time window, and given that the nearby-link approach assumes a constant transmitted power, we adjust the minimum received power $\mathrm{P_{min}}$ as $\mathrm{RSL_{min}} - (\mathrm{TSL_{max}} - \mathrm{TSL_{min}})$, similar to Roversi et al. (2020). Indeed, in our data set, ATPC (see section 2.2) was applied for many links. Note that this correction for ATPC assumes that $\mathrm{TSL_{max}}$ coincides with $\mathrm{RSL_{min}}$ during the 15-minute sampling period and therefore that the transmitted power instantly increases in response to a drop in received power due to rain. This assumption may not be entirely valid, as it would be reasonable to assume a certain response time. However, we leave such alternative approaches for future work. This permutation is referred to as NCI and includes the outlier filtering described in Section 3.1.

A third wet-dry classification method was used specifically for situations where accurate radar information is available. The objective of our research is to determine whether we can improve QPE using CML data, even when a dense rain gauge and radar network is available. In such cases, the occurrence of rain can be fairly accurately derived from the available radar information. Indeed, while radar faces challenges with accurate quantitative estimates, it detects the location and timing of rainfall with fairly high accuracy (Goudenhoofdt et al., 2017). In this third wet-dry classification method, a CML record was considered wet

https://doi.org/10.5194/egusphere-2026-457
Preprint. Discussion started: 5 March 2026

if at least one pixel of RAD-QPE indicated more than 0.1 mm h^{-1} of rain along the CML path length. RAD-QPE can be made available in near-realtime for nowcasting purposes. This experiment is referred to as RCI.

3.3 Wet-Antenna Attenuation

In addition to determining the baseline dry attenuation using the wet-dry classification outlined in the previous section, a correction must be made for attenuation due to water droplets on the antennas during rain events (wet-antenna attenuation, $\mathrm{A_{waa}}$, see Equation 1). Several methods exist for this correction, and we applied three different approaches to our CML data.

First, as suggested by Overeem et al. (2016a), we tested a constant value for the $\mathrm{A_{waa}}$ of 2.3 dB (experiment RCI, which is identical to the final experiment described in the previous section).

A second experiment (RTI) uses the time-dependent method of Schleiss et al. (2013), which also assumes a maximum $\mathrm{A_{waa}}$ of 2.3 dB during wet periods, but allows for an exponential increase during the early stages of rainfall and an exponential decrease after the end of a rainfall event. The typical time scale for the $\mathrm{A_{waa}}$ to decrease by 95 % is about 15 minutes, which is also the resolution of the CML data in our study. Note that this method generally performs better for high-temporal-resolution ($<$ 15 minutes) CML data (Pastorek et al., 2022).

Pastorek et al. (2022) demonstrated that models assuming a constant $\mathrm{A_{waa}}$ or a time-varying $\mathrm{A_{waa}}$ are outperformed by models with rainfall intensity dependence. They propose such a method, similar to Leijnse et al. (2008), in which $\mathrm{A_{waa}}$ increases according to a power law relative to the measured attenuation A, but with an upper limit for $\mathrm{A_{waa}}$ of 14 dB. This experiment is referred to as RII.

3.4 Fitting of Specific Attenuation - Rain Rate Relation

A final experiment focuses on optimizing the relation between specific attenuation (corrected for baseline attenuation and wet antennas) and rain rate, similar to e.g. van Leth et al. (2018); Overeem et al. (2016a), with a special focus on the frequency dependence. The default method, typically used in CML research, employs the International Telecommunication Union relation as described in (ITU, 2005). This recommendation provides typical attenuation rates for a range of microwave frequencies and rainfall intensities based on global rainfall observations. Rainfall properties, such as the typical drop size distribution, might deviate from these global average conditions in the mild, maritime climate of Belgium. Therefore, taking advantage of three disdrometers that have been recording rainfall over several years at multiple locations in Belgium, experiment RID uses adjusted $\gamma - \mathrm{R}$ relations.

For all three disdrometers, we calculated the purely theoretical specific attenuation γ associated with their native-resolution raindrop size distributions, following e.g. Nebuloni et al. (2022):

$$\gamma(f,\mathrm{pol}) = \frac{4.343 \times 10^{-5}}{\Delta t} \sum_{i=1}^{N_D} \frac{C(D_i, f, \mathrm{pol})}{Area_i} \left(\sum_{j=1}^{N_V} \frac{n_{i,j}}{V_j}\right), \tag{4}$$

https://doi.org/10.5194/egusphere-2026-457
Preprint. Discussion started: 5 March 2026

where $\mathrm{Area_i}$ is the effective sampling area ($\mathrm{m^2}$) of the disdrometer (adjusted for drop size), $\Delta\mathrm{t}$ is the sampling time (s), $\mathrm{D_i}$ is the drop diameter (mm) of bin i, $\mathrm{V_j}$ is the drop velocity ($\mathrm{m\,s^{-1}}$) of bin j, and $\mathrm{n_{ij}}$ is the number of drops in size bin i and velocity bin j. The extinction cross section for a particular drop size, microwave frequency f, and polarization p, $\mathrm{C(D_i, f, pol)}$ ($\mathrm{mm^{-2}}$), is calculated using the T-matrix method via the pytmatrix Python package (Leinonen, 2014) to account for non-spherical raindrop shapes. When the T-matrix method fails to converge (typically for very large drops or high microwave frequencies), Mie theory is employed as a fallback, assuming spherical particles (Prahl, 2026). The calculation of γ was performed only for the summer months (June, July, and August) of 2024 and 2025 for all three disdrometers. This ensures a balanced dataset for the three instruments. As customary in disdrometer analyses (Raupach and Berne, 2015), all disdrometers were filtered for non-physical combinations of velocity and drop size. To do so, we allowed for deviations up to 25 % along the diameter and velocity axes compared to the Beard (1976) relation, with a minimum deviation of 1 mm or 1 $\mathrm{ms^{-1}}$ respectively. Only instances with pure liquid precipitation METAR codes reported by the disdrometers were included. In addition, we implemented a quality check by calculating the instantaneous rainfall rates from the drop size distribution, using:

$$R = \frac{6\pi \times 10^{-4}}{\Delta t} \sum_{i=1}^{N_D} \frac{N_i D_i^3}{Area_i}, \tag{5}$$

where R is the rain rate (mm $\mathrm{h^{-1}}$) and $\mathrm{N_i}$ is the number of drops in size bin i. If the rain rates calculated from the drop size distribution deviated by more than 25% from the rain rates reported by the disdrometer, we omitted that time stamp from further analysis.

Subsequently, we fitted parameters a and b in Equation 2 using values obtained of γ and R from Equations 4 and 5. Theoretical calculations of $\gamma(\mathrm{f, pol})$ were performed at 5 GHz intervals for all frequencies from 10 to 85 GHz and horizontal and vertical polarizations. A linear interpolation was applied for intermediate frequencies. Experiment RID employs the fitted relation averaged over the three Belgian disdrometers, shown for a few frequencies and horizontal polarization in Figure 3. These newly fitted parameters were then used in pycomlink to obtain rainfall for each CML, instead of the original ITU relations, using the appropriate microwave frequency and polarization as obtained from the CML metadata.

From Figure 3, the observed relations generally align with the ITU relations, although certain deviations are evident. For low frequencies, the three disdrometers suggest lower γ for extreme rainfall than the ITU relation. Conversely, for higher microwave frequencies, the observed relations suggest higher γ for extreme rainfall than the ITU relation. The three disdrometers generally agree well with one another, although the Uccle disdrometer tends to be slightly closer to the ITU relation than the other two disdrometers. Given that the three disdrometers are from different brands, this agreement offers reassurance that the new relations are robust for the Belgian climate. The deviation from the ITU relations is likely caused by the typically narrower drop size distributions and smaller drops in this maritime climate, compared to globally averaged rainfall conditions.

It is important to note that previous studies also re-fitted the relation between rainfall and attenuation. For example, Overeem et al. (2016a) showed this for a climate similar to that in our study in the neighboring country of The Netherlands. They fitted the inverse relation R-γ, rather than the γ-R relation fitted here (which is used in the pycomlink software). To allow for a comparison against Overeem et al. (2016a), Table 3 also shows the fits of this inverse R-γ relation for ITU (2005) and for the

https://doi.org/10.5194/egusphere-2026-457
Preprint. Discussion started: 5 March 2026

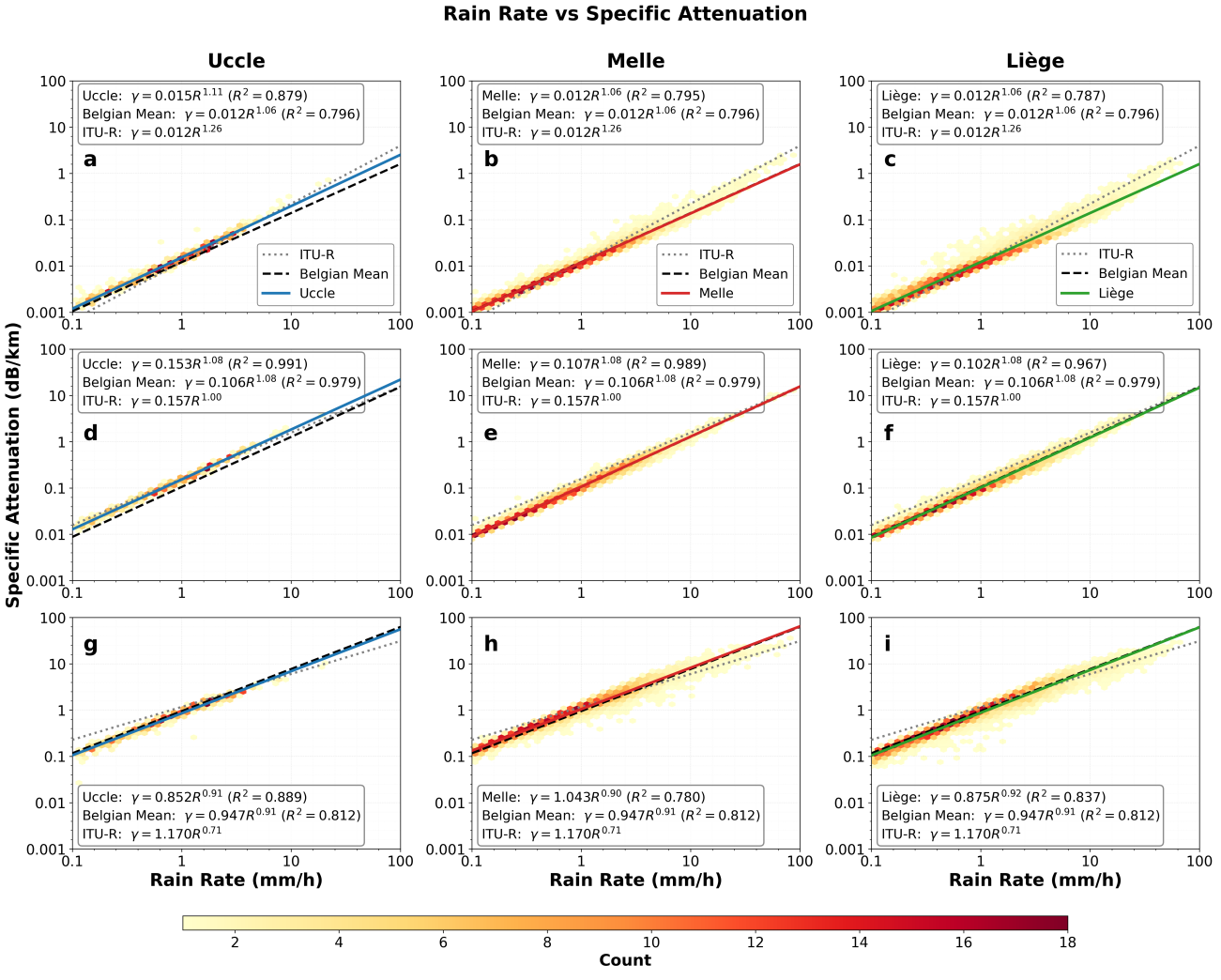

Figure 3. Fitting of the rain rate - specific attenuation relation based on the (left) Uccle, (middle) Melle and (right) Liège disdrometers for (1st row) 10 GHz, (2nd row) 25 GHz and (3rd row) 80 GHz assuming vertical polarization, based on the June, July and August observations from 2024 and 2025. The dotted line in each plot shows the ITU relation (ITU, 2005) for each frequency, the dashed line shows the mean of the fitted relation through the three Belgian disdrometers, and the colored line in each panel shows the fitted relation through the respective disdrometer data shown. Data is shown as a density with each dot representing the number of observations as shown in the color bar. Each panel shows the fitted relation for the disdrometer shown, as well as the three disdrometers averaged, and the ITU γ-R relation in the boxes.

https://doi.org/10.5194/egusphere-2026-457
Preprint. Discussion started: 5 March 2026

Table 3. Overview of the γ - R relation parameters, a ($\mathrm{dB\ km^{-1}(mm\ hr^{-1})^{-b}}$) and b (unitless) (Equation 2), according to ITU (2005) and as calculated from the average of the three disdrometers in Belgium for frequencies of 10, 25 and 80 GHz. We also show the inverse relation ($R-\gamma$) parameters, $\mathrm{a^{-1/b}\ (mm\ hr^{-1}(km\ dB^{-1})^{b}}$) and $\mathrm{1/b}$ (unitless), which can be directly compared to parameters a and b respectively in Figure 2 of Overeem et al. (2016a).

	ITU		Belgium	
Frequency	a	b	a	b
10 GHz	0.012	1.26	0.012	1.06
25 GHz	0.157	1.00	0.106	1.08
80 GHz	1.170	0.71	0.947	0.91
	ITU		Belgium	
Frequency	$a^{-1/b}$	$1/b$	$a^{-1/b}$	$1/b$
10 GHz	33.45	0.79	64.92	0.94
25 GHz	6.37	1.00	7.99	0.93
80 GHz	0.80	1.41	1.06	1.10

Belgian disdrometers. It is clear that the fits proposed in our study align well with Overeem et al. (2016a), with generally larger values for $\mathrm{a^{-1/b}}$ than in the ITU (2005) relation across all frequencies, and generally smaller values for $\mathrm{1/b}$ than ITU (2005), apart from for low frequencies.

4 Results

4.1 Outlier Filtering

Figure 4 compares the accumulated rainfall for Case 1 according to RAD-QPE, rain gauges, and the different CML retrievals. The latter two have been interpolated to the RAD-QPE grid with ordinary kriging, using a daily-varying climatological spherical variogram obtained from 30 years of rain gauge data in The Netherlands (Overeem et al., 2016a; van de Beek et al., 2012). All CML-derived rainfall data are treated as point measurements centered between the two antennas.

Interpolating the rain-gauge accumulations (Figure 4b) captures the general patterns shown by RAD-QPE. Additional statistics for all cases are provided in Table 4. From this table, the rainfall amounts from the gauges agree fairly well with RAD-QPE for Case 1, but larger deviations exist for the other cases (particularly Case 2 and 3). For Case 1 and 2, the interpolation of the rain gauge accumulations also produces smoother fields than those shown by radar, as reflected in the larger decorrelation length scale λ. This length scale is calculated as the e-folding radius (distance where the radially averaged 2D spatial correlation drops to 1/e) computed via Fast Fourier Transform-based autocorrelation (Table 4).

The first iteration of CML-derived rainfall (SCI-U) exhibits clear outliers with very high accumulations, evident from Figure 4c. This also results in excessive rainfall extremes (highest 99th percentile) across all cases and low λ values (Table 4). Removing these outliers using our independent-link outlier filtering and omitting any time steps with errored seconds (see Section

https://doi.org/10.5194/egusphere-2026-457
Preprint. Discussion started: 5 March 2026

3.1; SCI) substantially improves the rainfall extremes and decorrelation scales but also leads to a substantial underestimation of the mean accumulations across all cases by approximately 50%. The number of outliers removed in SCI is generally small (about 2-3%) and of the same order of magnitude as the number of CMLs removed (before outlier filtering) by the quality flags indicating errored seconds (1-2 % of the CMLs).

Table 4. Precipitation metrics (Spatial mean, Standard Deviation (Std), Spatial 99th Percentile (P99) and Autocorrelation Length Scale (λ) for different rainfall products across all cases. λ is the e-folding radius (distance where the radially-averaged 2D spatial correlation drops to 1/e) computed via Fast Fourier Transform-based autocorrelation. The gauges and all permutations of the CML-derived rainfall were regridded to the RAD-QPE grid using ordinary kriging (see text). **Bold** values indicate the largest value for each metric; *italic* values indicate the smallest value.

Metric	RAD-QPE	Gauges	SCI-U	SCI	NCI	RCI	RTI	RII	RID
Case 1									
Mean (mm)	**24.9**	23.2	24.8	*16.7*	18.3	18.3	19.0	24.2	24.0
Std (mm)	*13.1*	15.4	**21.3**	15.4	16.9	16.5	16.9	17.3	15.9
P99 (mm)	*53.3*	59.9	**98.3**	72.8	82.4	79.9	82.2	82.6	72.3
λ (km)	42.0	**46.0**	33.0	*29.0*	31.0	33.0	33.0	36.0	38.0
Case 2									
Mean (mm)	**9.3**	2.9	7.3	3.4	*2.5*	3.3	3.5	8.1	9.0
Std (mm)	7.4	*2.5*	**10.6**	3.5	3.1	3.6	3.6	4.5	4.5
P99 (mm)	32.2	*10.0*	**46.2**	14.5	12.1	15.0	15.4	21.5	22.0
λ (km)	24.0	**29.0**	*13.0*	22.0	24.0	20.0	20.0	16.0	14.0
Case 3									
Mean (mm)	**23.6**	18.6	19.9	14.9	14.8	*13.3*	13.8	20.1	20.1
Std (mm)	12.5	11.9	**18.0**	13.4	14.1	*11.7*	12.0	13.9	12.9
P99 (mm)	53.9	46.8	**67.8**	52.7	53.1	*44.3*	45.6	52.7	48.8
λ (km)	**41.0**	38.0	*36.0*	39.0	**41.0**	39.0	40.0	**41.0**	**41.0**
Case 4									
Mean (mm)	25.4	**29.7**	18.2	12.5	12.7	*10.5*	11.0	20.1	21.0
Std (mm)	11.9	13.1	**15.4**	7.1	8.4	*5.8*	6.0	8.0	8.1
P99 (mm)	58.2	66.9	**82.3**	36.3	45.9	*29.8*	30.8	41.9	40.9
λ (km)	**37.0**	36.0	*11.0*	12.0	14.0	13.0	13.0	18.0	23.0
Case-average									
Mean (mm)	**20.8**	18.6	17.6	11.9	12.1	*11.4*	11.8	18.1	18.5
Std (mm)	11.2	10.7	**16.3**	9.8	10.6	*9.4*	9.6	10.9	10.4
P99 (mm)	49.4	45.9	**73.6**	44.1	48.4	*42.2*	43.5	49.7	46.0
λ (km)	36.0	**37.2**	*23.2*	25.5	27.5	26.2	26.5	27.8	29.0

https://doi.org/10.5194/egusphere-2026-457
Preprint. Discussion started: 5 March 2026

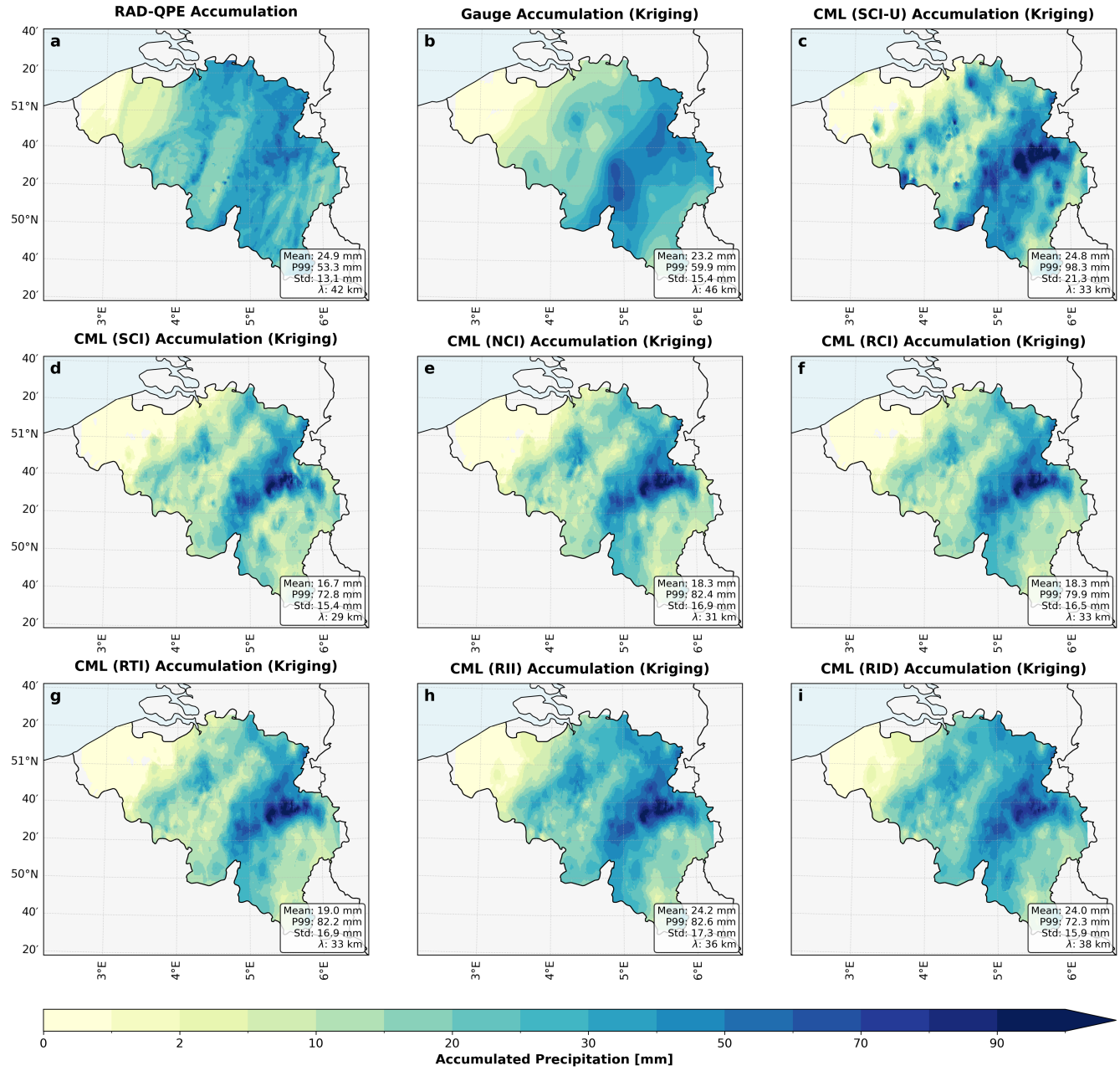

Figure 4. Accumulated rainfall during Case 1 as obtained using the RAD-QPE (a) and as regridded to the 1 km RAD-QPE grid using all rain gauges (b), and all permutations of the CML retrievals (c-i). Some statistics on the accumulations are provided in the box in each panel (see Table 4 for explanation about these metrics).

https://doi.org/10.5194/egusphere-2026-457
Preprint. Discussion started: 5 March 2026

Given the variable spatial data density of the different rainfall products, an objective evaluation is performed at the locations of the gauges only, using the gauges as a reference. To this end, Figure 5 shows scatter plots of case-total gauge-accumulations at each rain gauge location (Figure 1b) against the RAD-QPE and CML-derived rainfall accumulations. Table 5 provides statistcs for all cases. The RAD-QPE values in Figure 5a represent the average of all radar grid points within 2.5 km of the respective gauge location. The CML values in this figure represent the average of all CMLs having their midpoints within 2.5 km of the respective gauge location. Only rain gauges with valid data across all data sources were retained in the scatter plots to have identical sample sizes in each panel. Note that the rain gauges and RAD-QPE are not entirely independent, since many of the station networks were used in the adjustment of the radar fields in RAD-QPE (see Section 2.4). However, RAD-QPE was constructed for 5-minute accumulations and then aggregated, and no additional adjustment towards case-total accumulations was performed. In addition, the stations from the IBGE network were not included in the construction of RAD-QPE.

At the gauge locations, RAD-QPE exhibits larger accumulations than the gauges (Figure 5a), consistent with the earlier spatial analysis. This positive bias is consistent across Cases 1, 2 and 3 (Table 5). The unadjusted CML retrievals (SCI-U) exhibit a reduced bias (apart from Case 3; Figure 5b and Table 5) but typically larger RMSE and smaller R^2 compared to RAD-QPE. Particularly the extremes seem overestimated in SCI-U (Figure 5b). Removing the outliers and erroneous links from the dataset (SCI; Figure 5c and Table 5) reduces the RMSE and increases the R^2 but introduces an overall negative bias.

4.2 Wet-Dry Classification

A first optimization of the CML rainfall retrieval concerns the wet-dry classification. This classification is needed to determine the baseline attenuation during dry conditions. In addition, the wet-dry classification prevents rainfall to be detected during dry periods from attenuation unrelated to precipitation. As outlined in Section 3.2, we implement three techniques, each described previously in literature (the rolling standard deviation approach (SCI), the nearby-link approach (NCI) and the RAD-QPE-based approach (RCI)). To help understand the impact of the wet-dry classification, Figure 6 shows time series for the (left) overall and baseline attenuation, (middle) wet-antenna and rainfall attenuation, and (right) the retrieved rainfall intensity, for three randomly selected microwave links with low (top), medium (middle) and high (bottom) frequency, during a section of Case 1. Only CMLs with their midpoint in the vicinity (2.5 km) of a rain gauge were chosen for comparison.

From this figure, it is evident that the three tested methods identify considerably different wet periods, particularly for the mid- and high-frequency links (Figure 6d and g). SCI classifies the early afternoon of 22 June as mostly dry, whereas persistent light rainfall (order a few $\mathrm{mm\ hr^{-1}}$) was recorded in the RAD-QPE and nearby gauges during that time (Figure 6f). Note that for a typical 25 GHz link with a length of 4 km, the minimum detectable rainfall (given the precision of 1 dB), would be about $1\ \mathrm{mm\ hr^{-1}}$. The periods of more substantial peak precipitation, e.g. in the low-frequency link (Figure 6a) or around 10 UTC in the other links (Figure 6d and g), are correctly identified by all methods. The fact that rainfall periods with low intensity and low variability can be missed by the rolling standard deviation method may contribute to the general underestimation observed in SCI compared to both RAD-QPE and the rain gauges, as shown in the previous section.

https://doi.org/10.5194/egusphere-2026-457
Preprint. Discussion started: 5 March 2026

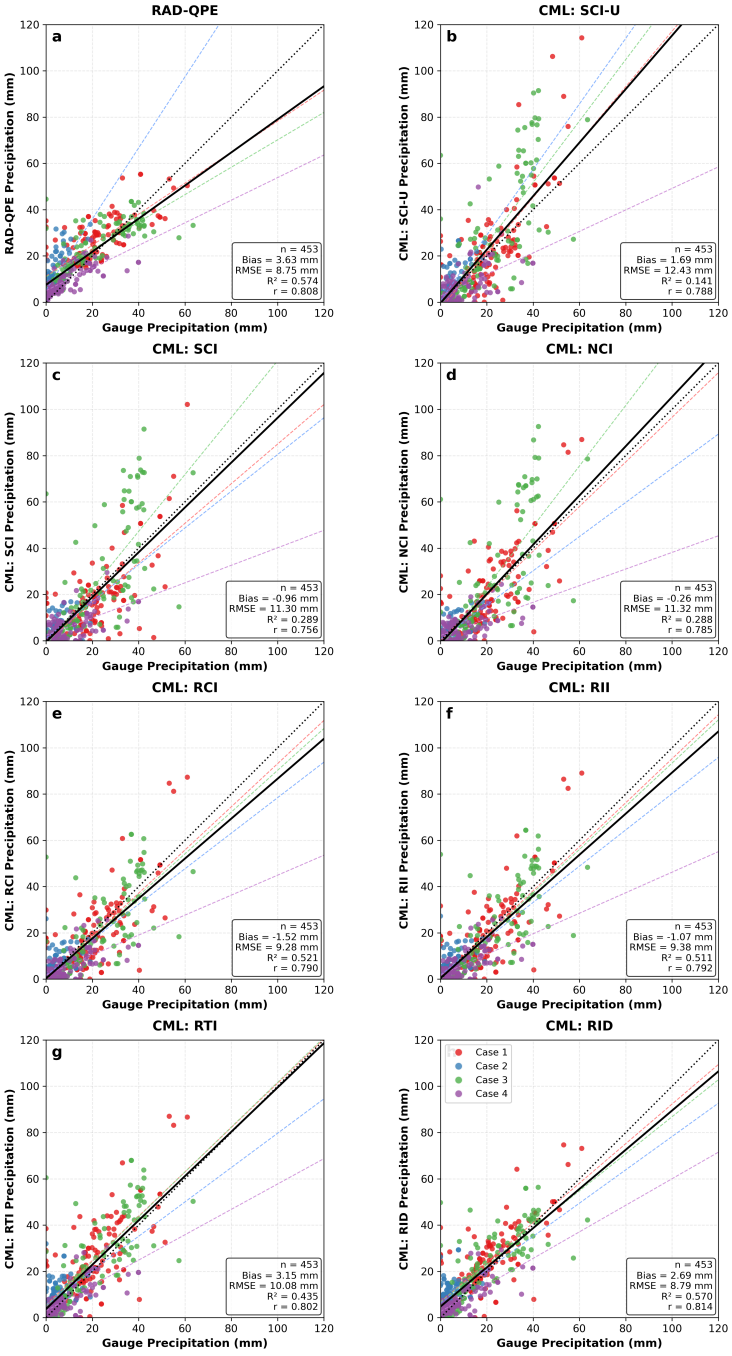

Figure 5. Scatter plots of case-accumulated rainfall from the rain gauges versus (a) the RAD-QPE, and (b-i) all permutations of CML-rainfall retrievals for all cases. The colors denote the different cases represented as shown in the legend. Only gauges that have valid data for all products are considered. For RAD-QPE, all grid points within 2.5 km of the gauges were averaged, while for the CML, all links with midpoints within 2.5 km of the gauges were averaged. The black dotted line shows the 1:1 relation, while the colored dashed lines show a linear regression through each case separately. The black line shows a linear regression through all points combined. Each panel shows some statistics, including the number of data points (n), the mean bias (bias), the Root Mean Squared Error (RMSE), the coefficient of determination (R^2), and the correlation (r), using the rain gauges as a reference.

https://doi.org/10.5194/egusphere-2026-457
Preprint. Discussion started: 5 March 2026

Table 5. Statistical comparison of precipitation estimates against gauge observations for RAD-QPE and the different permutations of the CML-derived rainfall, for each case separately. Shown are the absolute bias (Bias), the relative bias (Rel. Bias), the Root-Mean Squared Error (RMSE), the coefficient of determination (R^2) and the correlation (r). For RAD-QPE, all grid points within 2.5 km of the gauges were averaged, while for the CML, all links with midpoints within 2.5 km of the gauges were averaged. **Bold** values indicate best performance for each metric; *italic* values indicate worst performance.

Metric	RAD-QPE	SCI-U	SCI	NCI	RCI	RTI	RII	RID
Bias (mm)	4.4	1.4	-3.6	**-0.6**	-1.5	-0.8	*4.7*	3.8
Rel. Bias (%)	21.3	6.9	-17.5	**-3.1**	-7.5	-4.1	*22.6*	18.2
RMSE (mm)	**10.04**	*13.57*	12.29	11.65	11.54	11.70	12.88	10.88
R^2	**0.45**	*0.00*	0.18	0.27	0.28	0.26	0.10	0.36
r	0.76	**0.78**	*0.71*	0.75	0.74	0.74	0.74	0.76
Case 2								
Bias (mm)	*7.1*	2.0	0.4	**-0.2**	0.9	1.1	4.6	5.3
Rel. Bias (%)	*214.7*	61.7	12.6	**-6.0**	27.1	33.0	140.8	162.4
RMSE (mm)	*8.85*	5.25	3.72	**3.12**	4.25	4.41	6.96	7.27
R^2	*-4.61*	-0.98	0.01	**0.30**	-0.29	-0.40	-2.47	-2.79
r	**0.76**	**0.76**	0.63	0.68	0.58	0.57	*0.48*	0.49
Case 3								
Bias (mm)	2.5	*5.4*	2.8	3.4	-2.0	**-1.3**	4.2	2.6
Rel. Bias (%)	12.0	*26.1*	13.6	16.6	-9.7	**-6.3**	20.3	12.7
RMSE (mm)	**9.43**	*18.39*	16.83	17.43	11.71	11.85	12.25	10.02
R^2	**0.59**	*-0.58*	-0.32	-0.42	0.36	0.34	0.30	0.53
r	0.78	0.75	*0.74*	0.76	0.76	0.76	0.78	**0.79**
Case 4								
Bias (mm)	**0.1**	-2.4	-3.6	*-3.9*	-3.7	-3.5	-1.4	-1.4
Rel. Bias (%)	**1.3**	-25.3	-38.0	*-40.8*	-38.3	-36.2	-14.5	-15.1
RMSE (mm)	5.85	*8.14*	7.91	7.96	7.46	7.34	6.14	**5.82**
R^2	**0.55**	*0.13*	0.18	0.17	0.27	0.29	0.50	**0.55**
r	0.75	*0.55*	0.59	0.61	0.67	0.67	0.73	**0.76**
Overall (All Cases)								
Bias (mm)	*3.6*	1.7	-1.0	**-0.3**	-1.5	-1.1	3.1	2.7
Rel. Bias (%)	*26.7*	12.4	-7.1	**-1.9**	-11.2	-7.8	23.1	19.8
RMSE (mm)	**8.75**	*12.43*	11.30	11.32	9.28	9.38	10.08	8.79
R^2	**0.57**	*0.14*	0.29	0.29	0.52	0.51	0.44	**0.57**
r	**0.81**	0.79	*0.76*	0.78	0.79	0.79	0.80	**0.81**

https://doi.org/10.5194/egusphere-2026-457
Preprint. Discussion started: 5 March 2026

The difference between the nearby-link approach (NCI) and the radar approach (RCI) is smaller for the selected links (Figure 6a, d, and g), and agree better with the rainfall reported by the RAD-QPE and the gauges (Figure 6c, f, and i), although NCI exhibits somewhat more persistent wet periods.

This is also confirmed by the gridded rainfall maps in Figure 4 for Case 1. NCI and RCI both exhibit substantially more rainfall than SCI, bringing them closer to RAD-QPE and the gauges. In contrast, for Case 3 and 4 (Table 4), RCI exhibits a substantial dry bias compared to RAD-QPE and the rain gauges and underperforms compared to SCI. In contrast to Case 1 and 2, Case 3 and 4 are characterized by scattered showers, rather than widespread rainfall. Hence, slight mismatches between the timing of the radar and the CML performance records could lead to a less accurate wet-dry classification in these cases. In addition, as will be shown in the next section, there is an additional bias from the constant wet antenna correction in these three permutations, that could also be the culprit for NCI and RCI underestimations in Case 3 and 4, as there will be frequent wetting and drying of the antennas during scattered showers. Note that such a misrepresentation of wet and dry periods results in larger baseline attenuation estimation and missing some precipitation episodes, both of which reduce the estimated rainfall amounts.

Comparing the rainfall accumulations from the three wet-dry classification methods against the rain gauges in Figure 5 and Table 5 confirms that NCI has the lowest bias of the three methods, whereas RCI exhibits the best RMSE and R^2 of the three methods. Therefore, the permutations in the next sections will use the radar-based wet-dry classification.

4.3 Wet-Antenna Correction

In addition to identifying wet and dry periods, and the baseline attenuation, it is also important to correct for wet antennas during rain events. As outlined in Section 3.3, several methods exist to determine the wet-antenna attenuation, and three methods are tested in this study. The method applied in all permutations discussed thus far uses the fixed correction term as in Overeem et al. (2016a) (RCI). In addition, two dynamic methods were tested: a time-dependent (RTI) and intensity-dependent (RII) method. These three configurations use the same outlier filtering and the radar-based wet-dry classification, and their only difference consists of the wet-antenna correction approach.

The rain events around 10 UTC in the mid- and high-frequency link in Figure 6e and h clearly illustrate the different dynamics of the wet-antenna correction following the three methods. RCI always assumes a A_{waa} of 2.3 dB regardless of timing or intensity. This method therefore reduces the rain attenuation (A) more than the other methods at the start of the rain events. RTI uses a logarithmically increasing A_{waa}, saturating at 2.2 dB after some time (with a typical time scale of about 15 minutes; see Section 3.3). Given that this time scale equals the temporal resolution of our data, the difference with the RCI method is small, with only a short delay in the increase of A_{waa} after the start of wet periods (Figure 6b, e and h). Note that the A_{waa} in Figure 6 is capped at the remainder of $TRSL - A_{dry}$. For both the RCI and RTI, this means that often, periods identified as wet still end up without rain due to the wet antenna correction being larger than $TRSL - A_{dry}$. This may be contributing to the large dry bias in these permutations (Table 5), which appears to be caused by missing lighter rain (e.g. Figure 4f and g). The RII method, in contrast, clearly scales with the overall attenuation intensity (and hence with rainfall

https://doi.org/10.5194/egusphere-2026-457
Preprint. Discussion started: 5 March 2026

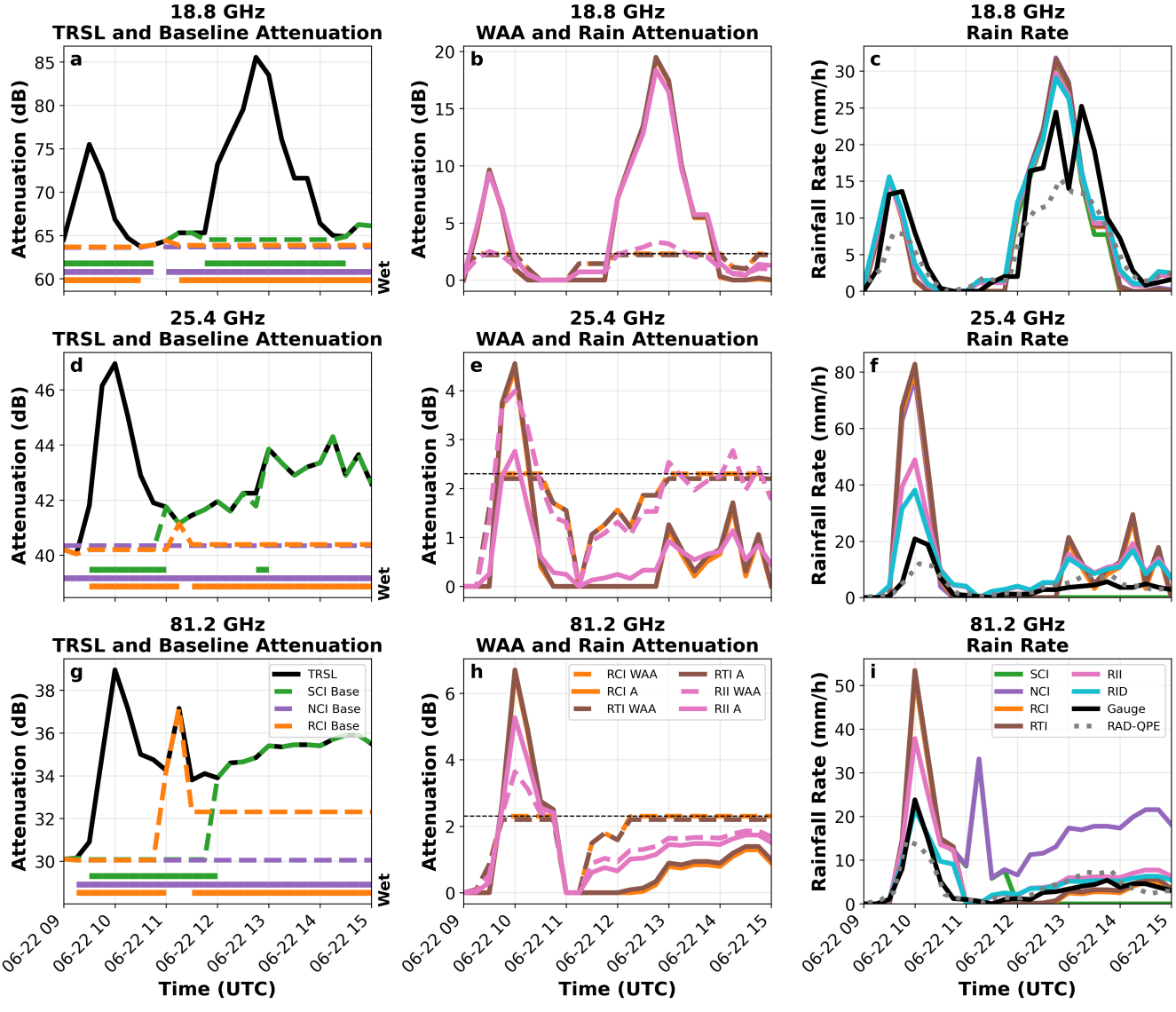

Figure 6. Time series of (left) the total (TRSL) and baseline (Base) attenuation, (middle) the wet-antenna (A_{waa}) and rainfall attenuation (A), and (right) retrieved rain rates for a low (top), mid (middle) and high (bottom) frequency CML within 2.5 km of a rain gauge, for 9 - 15 UTC on 22 June 2023. The colored bars in the left-hand panels indicate the periods identified as wet according to the various CML-retrieval algorithms. The colors correspond to the retrieval algorithms as shown in the legend. The faint, black dashed line in panels b, e and h denote the constant 2.3 dB A_{waa} that is used in RCI and RTI. For the 15-minute rain rates, the nearby rain gauge, RAD-QPE and the different CML retrieval algorithms are shown.

https://doi.org/10.5194/egusphere-2026-457
Preprint. Discussion started: 5 March 2026

intensity). Its wet-antenna correction is the largest among the three methods during the peak intensity around 10 UTC but smaller than RCI and RTI during lighter rain intensities at the start and end of the event.

This behavior is also reflected in the rainfall maps shown in Figure 4f, g and h and the overall statistics in Table 4. The CML-retrieved rainfall is persistently much higher in RII compared to RCI and RTI, bringing the values much closer to RAD-QPE and rain gauges.

From the more objective evaluation at the rain gauge locations (Figure 5 and Table 5), RII appears to have the worst metrics of the three wet-antenna correction methods, showing the largest positive bias, the smallest R^2, and the highest RMSE. RCI and RTI slightly underestimate the rainfall, while RII overestimates rainfall. However, note that RCI and RTI showed a substantial negative bias overall for the gridded product comparison in Table 4. It should be mentioned that the constant value of 2.3 dB could in principle be reduced in RCI and RTI, particularly during light rain, to allow more light rain to be detected.

4.4 Fitting of Specific Attenuation - Rain Rate Relation

A final optimization concerns the fitting of the relation between specific attenuation (γ) and rain rate (R) using observed summer drop size distributions in Belgium (Section 3.4). From Figure 4 and Table 4, it is evident that this fitting leads to a further improvement in RID compared to RII. Both experiments are identical apart from the γ-R relation, and both use the Pastorek et al. (2022) wet antenna correction, the radar wet-dry classification and outlier filtering. Note that combinations of the re-fitting of the $\gamma - R$ relation, combined with other options for the wet antenna correction and the wet-dry classification were tried, but that RID showed the best overall performance of all possible permutations (not shown). The overall accumulation statistics improve in RID compared to RII, particularly the extreme accumulations (Table 4).

This is also confirmed using the rain gauges as a benchmark (Figure 5 and Table 5). Overall, RID performs best of all permutations in terms of RMSE and R^2, and outperforms RAD-QPE in terms of the bias against the rain gauges, with other metrics very similar between RAD-QPE and RID.

As outlined in Section 3.4, primarily the low- and high-frequency links are influenced by the re-fitting of the γ-R relation, with increases and decreases in rain rates for a given γ, respectively, particularly during high-intensity events. This is also evident from the individual CML time series in Figure 6i. Particularly for the high-frequency link and for the intense rainfall event around 10 UTC, RID brings the rainfall intensity into closer agreement with the gauges (with the black and cyan line virtually overlapping).

To more systematically assess the impact on links with different frequencies, Figure 7 shows the evaluation of CMLs against rain gauges, disaggregated by low-, mid-, and high-frequency ranges. While RII clearly exhibits an underestimation of retrieved rain rates for the long, low-frequency CMLs and an overestimation for the short, high-frequency CMLs, the re-fitted retrievals in RID show improvements in all parameters for low-, mid-, and high-frequency links and more consistent behavior across frequencies.

https://doi.org/10.5194/egusphere-2026-457
Preprint. Discussion started: 5 March 2026

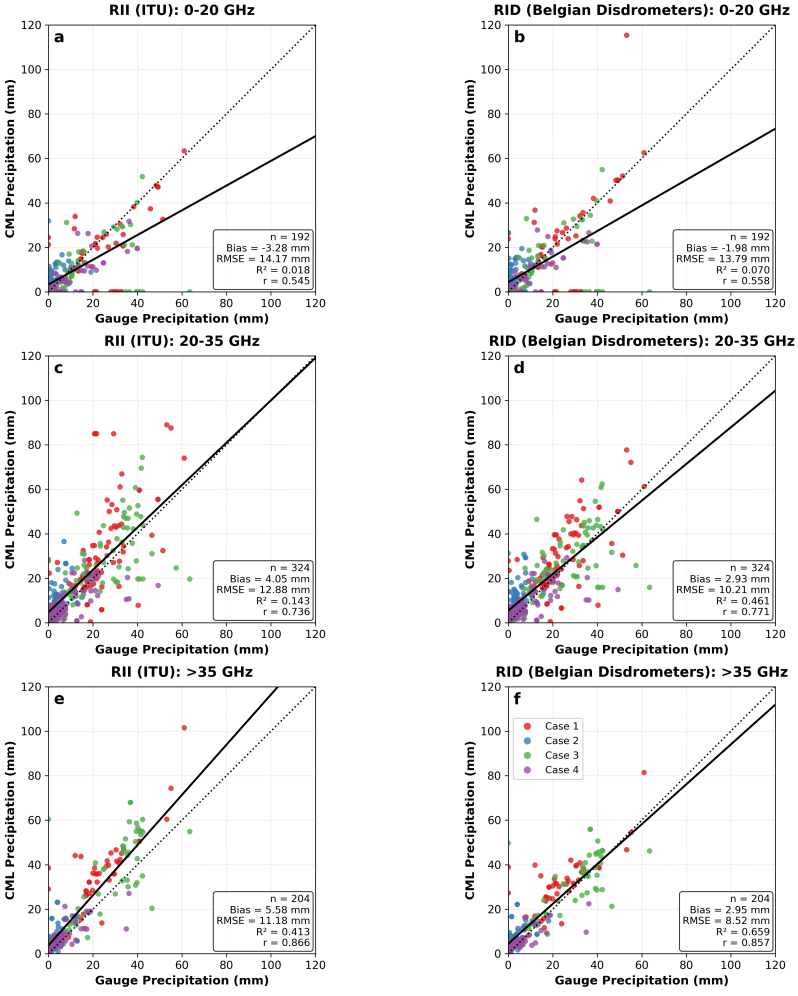

Figure 7. As Figure 5, but for the (left) RII and (right) RID experiments and for (top) low, (middle) intermediate and (bottom) high-frequency CMLs. Each panel shows some statistics, including the number of data points (n), the mean bias (bias), the Root Mean Squared Error (RMSE), the coefficient of determination (R^2), and the correlation (r), using the rain gauges as a reference.

https://doi.org/10.5194/egusphere-2026-457
Preprint. Discussion started: 5 March 2026

4.5 Case study of Brussels

Given that the RID retrieval shows substantial improvements particularly for high-frequency links, and given that the CML network consists of a high density of short, high-frequency links over several urban areas in Belgium (Figure 1a), it is instructive to focus our assessment on these urban areas. Indeed, urban rainfall-runoff modeling or inundation modeling benefits from high spatial resolution input data, which is difficult to capture effectively with C-band radars.

In the Brussels Capital Region (BCR), a dense, high-temporal-frequency rain gauge network exists that is independent of RAD-QPE. This allows for more in-depth evaluation over this area at 15-minute time scales. Table 6 shows the overall statistics for this network in Brussels for each of the cases considered in this study. High rainfall amounts were observed particularly for Case 1 and Case 3 in the BCR (Table 6).

Table 6. As Table 1, but for the IBGE network only, and including the average rain rates. Shown are the domain-average rain rate $\mathrm{mm\ hr^{-1}}$, the domain average intensity (rain rate during rain; $\mathrm{mm\ hr^{-1}}$), the case-total accumulation (mm) and the case-accumulated 99th percentile (mm) and standard deviation (mm).

Case	Mean Rate ($\mathrm{mm\ hr^{-1}}$)	Mean Intensity ($\mathrm{mm\ hr^{-1}}$)	Mean Accumulation (mm)	P99 (mm)	Std (mm)
Case 1	1.08	5.3	26.0	33.7	7.9
Case 2	0.11	6.5	5.4	13.0	3.2
Case 3	0.79	6.0	37.9	42.4	3.3
Case 4	0.11	4.8	5.1	7.7	1.6
Overall	0.44	5.7	18.6	42.3	14.7

The dense rain gauge and CML network in the BCR is evident from Figure 8b, c and d. This figure shows a snapshot of one of the most intense rainfall episodes observed across all cases, around 10:15 UTC during Case 1. An intense shower affected mainly the northwestern half of the BCR with rain rates exceeding 5 mm in 15 minutes, but lighter rain in the southeast of the BCR. RAD-QPE appears to underestimate the rainfall intensity in the northwest compared to the rain gauges, although the region in the north of the BCR with relatively weaker rainfall in RAD-QPE is not well covered by rain gauges. RII clearly overestimates the rain rates across the region, although the general pattern matches the gauges and RAD-QPE well. RID substantially reduces the rainfall intensities compared to RII and brings them much closer to those recorded by the gauges and RAD-QPE. It also shows more fine-scale structure than the other rainfall products over Brussels.

Figure 9 shows the 15-minute rainfall time series for all four cases, averaged over all IBGE gauge locations across the BCR area, using RAD-QPE, the IBGE gauge network, and all permutations of CML-derived rainfall. From this figure, RID systematically appears to outperform the other CML retrievals, particularly during the most extreme rainfall episodes. It also often performs better than RAD-QPE in terms of rainfall intensity, using the gauges as a benchmark.

A more systematic evaluation against the 15-minute accumulations from the IBGE rain gauges is shown in Figure 10 and in Table 7. Averaged over all cases, RID outperforms RAD-QPE in the urban area of Brussels in terms of RMSE, R^2 and correlation, and shows a very similar small overestimation of about 20 %.

https://doi.org/10.5194/egusphere-2026-457
Preprint. Discussion started: 5 March 2026

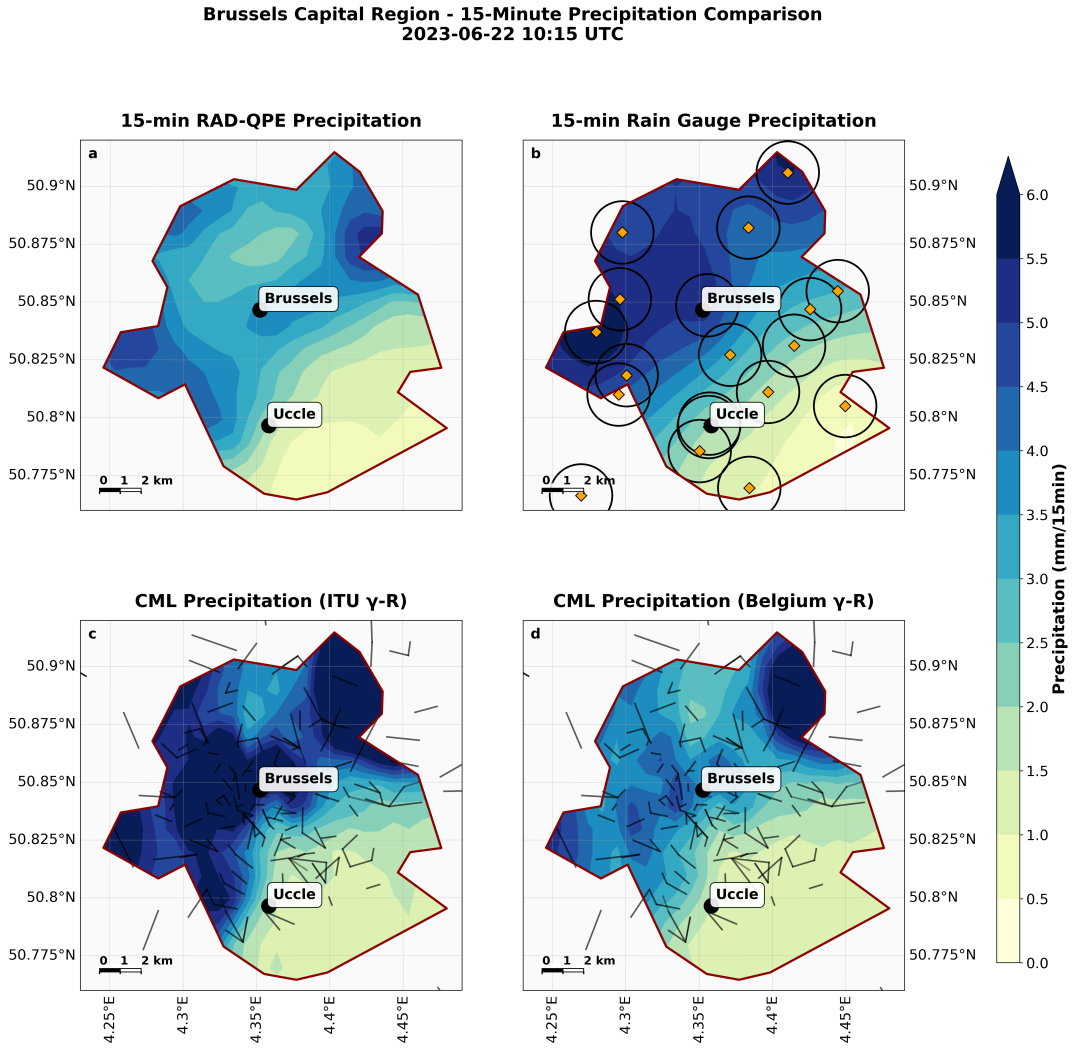

Figure 8. 15-min rainfall accumulation contour maps at 10.15 UTC on 22 June 2023, covering the Brussels Capital Region (BCR), as obtained from the (a) RAD-QPE, (b) IBGE rain gauge network, (c) RII CML retrieval and (d) RID CML retrieval. Only data within the BCR are shown and the brown outline denotes the border of the BCR. All data is regridded to the 1 km RAD-QPE grid using ordinary kriging. All gauge locations are indicated in panel b by orange diamonds and a circle of 2.5 km is drawn around them to focus on data that are not extrapolated too far from the gauges. Panels c and d also denote the locations of all CMLs in the BCR.

https://doi.org/10.5194/egusphere-2026-457
Preprint. Discussion started: 5 March 2026

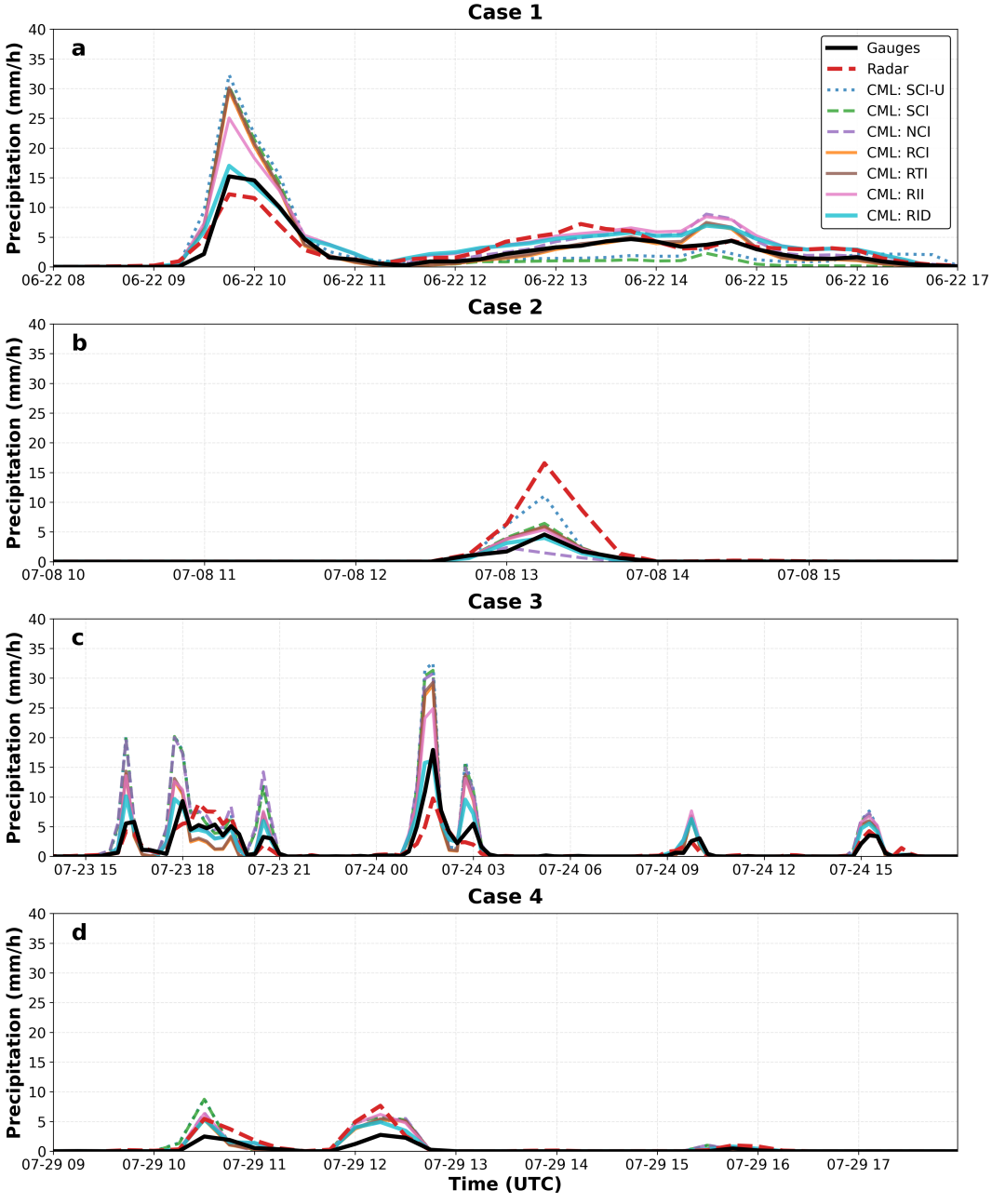

Figure 9. 15-minute rainfall times series for (a) Case 1, (b) Case 2, (c), Case 3 and (d) Case 4 within the Brussels Capital Region, as obtained from the average of the IBGE network, RAD-QPE and the several permutations of the CML retrievals. For RAD-QPE, all grid points within 2.5 km of the gauges were averaged, while for the CML, all links with midpoints within 2.5 km of the gauges were averaged for each of the gauges, prior to averaging over all 16 IBGE gauges.

https://doi.org/10.5194/egusphere-2026-457
Preprint. Discussion started: 5 March 2026

Table 7. As Table 5, but for 15-minute rainfall statistics across the IBGE gauge locations. For RAD-QPE, all grid points within 2.5 km of the gauges were averaged, while for the CML, all links with midpoints within 2.5 km of the gauges were averaged for each of the gauge comparisons, prior to averaging over all 16 IBGE gauges. **Bold** values indicate best performance for each metric; *italic* values indicate worst performance.

Metric	RAD-QPE	SCI-U	SCI	NCI	RCI	RTI	RII	RID
Case 1								
Bias (mm/hr)	0.33	0.27	**-0.06**	0.53	0.28	0.36	*0.76*	0.48
Rel. Bias (%)	27.9	22.8	**-5.2**	44.5	23.7	29.7	*63.4*	40.3
RMSE (mm/hr)	1.69	*3.34*	2.63	2.47	2.37	2.45	2.13	**1.67**
R^2	0.73	*-0.05*	0.35	0.42	0.47	0.43	0.57	**0.74**
r	0.86	*0.82*	0.85	0.89	0.88	0.89	**0.90**	0.88
Case 2								
Bias (mm/hr)	*0.28*	0.12	0.05	-0.05	0.03	0.03	0.03	**-0.00**
Rel. Bias (%)	*276.4*	118.3	48.2	-46.3	29.5	33.1	26.7	**-3.8**
RMSE (mm/hr)	*2.36*	1.73	1.02	1.11	0.99	0.99	0.93	**0.92**
R^2	*-2.01*	-0.62	0.44	0.33	0.47	0.47	0.53	**0.55**
r	**0.78**	0.72	0.75	*0.58*	0.74	0.74	0.76	0.74
Case 3								
Bias (mm/hr)	**-0.09**	0.75	0.71	*0.77*	0.22	0.26	0.36	0.12
Rel. Bias (%)	**-11.2**	91.1	85.9	*94.1*	26.9	31.9	44.2	14.6
RMSE (mm/hr)	**1.39**	*3.68*	3.53	3.51	2.64	2.72	2.22	1.43
R^2	**0.68**	*-1.22*	-1.05	-1.03	-0.15	-0.22	0.19	0.66
r	0.83	0.82	0.82	0.82	*0.81*	0.81	0.85	**0.86**
Case 4								
Bias (mm/hr)	0.06	*0.07*	0.06	0.05	**0.00**	0.01	0.03	0.01
Rel. Bias (%)	53.5	*63.1*	50.5	40.9	**4.3**	8.6	30.4	10.6
RMSE (mm/hr)	0.95	*1.34*	1.27	1.03	0.93	0.96	0.90	**0.68**
R^2	-1.03	*-3.07*	-2.64	-1.41	-0.97	-1.07	-0.82	**-0.05**
r	**0.65**	0.58	0.60	0.62	*0.57*	0.58	0.63	**0.65**
Overall (All Cases)								
Bias (mm/hr)	**0.09**	0.34	0.25	*0.35*	0.13	0.15	0.26	0.12
Rel. Bias (%)	**17.4**	64.9	48.6	*67.4*	24.2	29.4	49.7	23.1
RMSE (mm/hr)	1.54	*2.72*	2.45	2.38	1.92	1.98	1.67	**1.20**
R^2	0.46	*-0.69*	-0.37	-0.29	0.16	0.11	0.36	**0.67**
r	*0.74*	0.80	0.80	0.81	0.82	0.82	**0.85**	**0.85**

https://doi.org/10.5194/egusphere-2026-457
Preprint. Discussion started: 5 March 2026

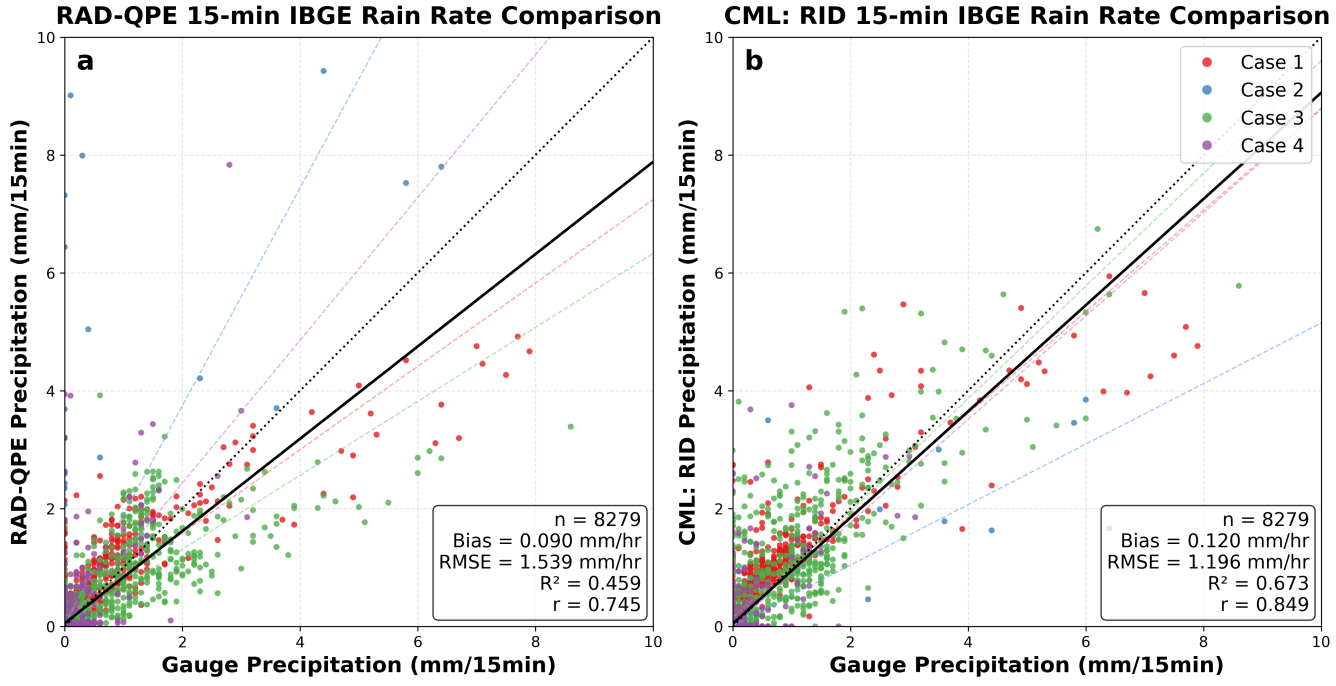

Figure 10. As Figure 5, but for the 15-minute rain rates in (a) RAD-QPE and (b) the RID CML retrieval. For RAD-QPE, all grid points within 2.5 km of the gauges were averaged, while for the CML, all links with midpoints within 2.5 km of the gauges were averaged for each of the gauges, prior to averaging over all 16 IBGE gauges.

5 Discussion

The results presented in the previous section highlight the potential of CML as an additional source of information for constructing high-quality, high-resolution rainfall products. Although the quality of RAD-QPE already meets high standards, as discussed in Journée et al. (2023), further improvements at high spatiotemporal scales would benefit warning systems for regional- or city-scale hydrological services and post-rainfall assessments for insurance claims. Such improvements would also benefit nowcasting of intense isolated storms (Imhoff et al., 2023) and detailed evaluation of numerical atmospheric models (Prudden et al., 2020; Sokol et al., 2021).

However, our results also reiterate the importance of careful processing of CML information, as previously suggested by, for example, Overeem et al. (2016a); Uijlenhoet et al. (2018); Chwala and Kunstmann (2019). When CML metadata include information about link signal quality, such as errored or unavailable seconds, this information, in addition to careful outlier detection, can be used to remove problematic links. This step is essential to eliminate erroneous rainfall amounts associated with malfunctioning links. When a high-resolution radar network is available, using this information for wet-dry classification can improve the retrievals, as demonstrated by our results. This method exhibits slightly better performance compared to using the nearby-link approach or a rolling standard deviation. This is consistent with earlier findings of Overeem et al. (2016b).

https://doi.org/10.5194/egusphere-2026-457
Preprint. Discussion started: 5 March 2026

The rolling standard deviation appears sensitive to missing rainfall during persistent light rain episodes and has been shown by earlier studies to be more appropriate for datasets with higher temporal frequency (e.g., Graf et al. 2020) than in our dataset. While the use of radar outperformed other methods of wet-dry classification, it should be noted that rainfall could still be missed due to timing errors or issues typical of radar-rainfall estimation (near-surface evaporation, blocking, etc.).

In addition, we demonstrate that quantifying the attenuation associated with wet antennas is critical for quantitative precipitation estimation from CMLs. We confirm the findings of Pastorek et al. (2022) that a correction proportional to rainfall intensity leads to more light rain being detected compared to using a constant or time-dependent correction. The latter two permutations resulted in a substantial dry bias in our retrievals, whereas the time-dependent correction was generally associated with an overestimation of rainfall. The constant value of 2.3 dB (to which also the time-dependent wet antenna attenuation asymptotes) could be re-calibrated for the network in this study, although given the underestimation of light rain and overestimation of intense rain in many of the cases in this study, a re-calibrated intensity-dependent wet-antenna correction may be more promising. It should also be mentioned that considerable uncertainty on the wet-antenna correction exists due to the fact that both antennas of a CML are not necessarily wet at the same time, particularly during scattered showers.

Finally, our study robustly demonstrates that using the standard ITU relations for the conversion of attenuation to rain intensity leads to overestimations (underestimations) of intense rainfall for high- (low-) frequency CMLs. Re-fitting using summertime data from three disdrometers in Belgium consistently improves the rainfall retrievals for low- and high-frequency links. Previous studies either did not reveal substantial improvement through re-fitting against local disdrometers (van Leth et al., 2018) or showed more modest improvements than in our study (Overeem et al., 2016a), even for similar climates as in our study. However, van Leth et al. (2018) investigated only a single link at 38 GHz, while the network under investigation in Overeem et al. (2016a) consisted of CMLs with frequencies generally lower than 40 GHz. The dataset in this study contains many high-frequency links over cities, and we show that it is mainly the low ($<$20 GHz) and high ($>$75 GHz) frequency links that benefit from re-fitting against local disdrometer data. Indeed, for mid-frequency links, it is well known that the exponent of the γ-R relation is closer to one (e.g., Chwala and Kunstmann 2019). For urban areas with dense networks of short, high-frequency links (related to the higher communication load), proper fitting with local drop size distribution information is essential to capture extreme rainfall events.

Among all CML retrieval permutations tested here, the combination of careful outlier removal, radar-based wet-dry classification, rainfall-intensity-dependent wet-antenna correction, and a re-fitted γ-R relation substantially outperforms the other CML-retrieval methods. The quality of our nationwide, but particularly our city-scale, rainfall retrievals from CMLs approaches or exceeds those of a state-of-the-art radar-gauge merged product for locations with sufficient links in the vicinity. Although radar remains indispensable given its fairly complete geographical coverage, and a dense gauge network is required for proper ground-truth validation, our results provide evidence that existing multimodal rainfall products could be substantially improved through integration of CML information that can be accessed in real time. Future studies will explore the benefits of doing so based on our datasets. It is also important to note that all CML processing techniques employed in this paper are available in real time and could, in principle, be implemented operationally.

https://doi.org/10.5194/egusphere-2026-457
Preprint. Discussion started: 5 March 2026

A caveat of our study is that we included only a limited number of intense precipitation events as case studies. Longer studies including more diverse precipitation events are required for a more robust estimate of the quality of rainfall retrievals from CMLs. For instance, it is well known that winter precipitation is more challenging for QPE from CMLs Overeem et al. (2016b). Ultimately, for CML-derived rainfall to reach its full potential, real-time availability of city-scale or nationwide CML performance data will be essential. Fortunately, efforts are underway to facilitate such data provision by mobile network operators (Fencl et al., 2025).

6 Conclusions

This study evaluated the potential of commercial microwave link (CML) networks to complement existing rain gauge and weather radar observations in Belgium, a region with a very dense hydrometeorological observation network.

We analyzed four intense summer rainfall events in 2023 using over 2800 microwave (sub)links spanning frequencies from 10 to 85 GHz. Through systematic sensitivity experiments, we assessed the impact of various processing techniques on the quality of CML-derived rainfall estimates. Our findings demonstrate that careful data processing is essential for obtaining reliable rainfall estimates from CML networks. Specifically, we developed an outlier filtering algorithm that accounts for links sharing common antenna hubs. Furthermore, we showed that wet-dry classification using radar information somewhat outperformed methods based on rolling standard deviation or nearby links, particularly for persistent and lighter rainfall episodes. The choice of wet-antenna correction method proved critical, with rainfall-intensity-dependent corrections yielding rainfall overestimation, while constant or time-dependent corrections lead to rainfall underestimation.

Most significantly, our study demonstrates that re-fitting of the specific attenuation-rainfall relation using local disdrometer observations substantially improves rainfall retrievals, particularly for low-frequency (< 20 GHz) and high-frequency (> 75 GHz) links. The rainfall characteristics of Belgium's maritime climate are conducive to lower (higher) specific attenuation for extreme rainfall at low (high) frequencies compared to the global average relations provided by the International Telecommunication Union. This finding has important implications for urban areas, where dense networks of high-frequency links are common. In the Brussels Capital Region, our optimized CML-derived rainfall estimates outperformed a state-of-the-art radar-gauge merged product in terms of root mean square error, R^2, and correlation against independent rain gauge measurements at 15-minute temporal resolution, while biases were very similar.

These results provide compelling evidence that commercial microwave link networks can serve as a valuable complementary data source for multimodal precipitation estimation, particularly in urban environments where high-frequency link density is greatest. The fine spatial structure captured by CML observations, combined with their ability to measure rainfall close to the surface, offers advantages that complement the broader coverage of weather radar and the direct point measurements of rain gauges. Our study also highlights the importance of open-source software tools, for instance those made available through the OpenSense community and the Global Microwave Link Data Collection Initiative (GMDI) (Fencl et al., 2025; Graf et al., 2025), which have greatly facilitated the processing of CML data in this study.

https://doi.org/10.5194/egusphere-2026-457
Preprint. Discussion started: 5 March 2026

For future work, we recommend several avenues of investigation. First, longer-term studies encompassing a wider range of precipitation types and intensities are needed to more robustly characterize CML retrieval performance across different meteorological conditions (similar to e.g. Overeem et al. (2016b); Graf et al. (2020). Second, investigation of optimal methods for integrating CML information into existing multimodal QPE products, such as through data assimilation or multi-source blending techniques, would be valuable. Third, extension of the re-fitting to other climatic regions and seasons would help establish whether local drop size distribution information consistently improves retrievals. Fourth, dedicated experiments into how wet antennas attenuate CML signals are needed, particularly for lighter rainfall. Finally, establishing real-time data-sharing agreements with mobile network operators and developing operational processing chains will be essential for realizing the full potential of CML networks for hydrological applications and severe weather warning systems. The growing availability of CML data worldwide, combined with advances in processing techniques demonstrated in this study, suggests that commercial telecommunication infrastructure could play an increasingly important role in next-generation precipitation monitoring systems, especially in scarcely gauged regions.

Data availability. All rain gauge data and data from RAD-QPE are available from the RMI through their open data platform (https://opendata.meteo.be/) or via https://www.meteo.be/en/about-rmi/contact/contact-rmi. The disdrometer data are made available via the https://disdrodb.readthedocs.io/en/latest/ sharing platform. The commercial microwave link data are not shared with the wider community due to their business-sensitive nature, but data can be made available upon request by the corresponding author, after explicit agreement from Telenet N.V.

Author contributions. Kwinten Van Weverberg: conceptualization; formal analysis; software; validation; methodology; visualization; writing – original draft; writing – review and editing. Nina Neutens: formal analysis; software; validation; methodology. Simon De Corte: formal analysis; software; validation; methodology. Armani Passtoors: formal analysis; software; validation. Stephan Calderan: data provision and curation; methodology. Nicolas Ghilain: data provision and curation; methodology. Ricardo Reinoso-Rondinel: data provision and curation; methodology, writing – review and editing. Maarten Reyniers: data provision and curation, methodology, writing – review and editing. Hans Van de Vyver: writing – review and editing. Bert Van Schaeybroeck: writing – review and editing. Bart De Wit: data provision and curation. Aart Overeem: conceptualization; formal analysis; methodology; writing – review and editing. Remko Uijlenhoet: conceptualization; formal analysis; methodology; writing – review and editing.

Competing interests. The authors declare no competing interests

Acknowledgements. The authors are very grateful to Stephan Calderan and Stef De Ridder for sharing the Telenet N.V. network performance data. We also would like to acknowledge all contributors to the pycomlink, pytmatrix and miepython packages and the OpenSense community (https://opensenseaction.eu/) for sharing opensource tools and facilitating the data processing. The computational resources (Stevin

https://doi.org/10.5194/egusphere-2026-457
Preprint. Discussion started: 5 March 2026

Supercomputer Infrastructure) and services used in this work were provided by the VSC (Flemish Supercomputer Center), funded by Ghent
530 University, FWO and the Flemish Government – department EWI. K. Van Weverberg is funded by BELSPO project FED-tWIN2021-prf024 - ARCHWAy. The authors declare that AI tools (Claude.ai) was used to help with optimizing the data processing and refining the figures in this manuscript in Python.

https://doi.org/10.5194/egusphere-2026-457
Preprint. Discussion started: 5 March 2026

References

Beard, K. V.: Terminal Velocity and Shape of Cloud and Precipitation Drops Aloft, Journal of Atmospheric Sciences, 33, 851 – 864, https://doi.org/10.1175/1520-0469(1976)033<0851:TVASOC>2.0.CO;2, 1976.

Bellot, H., Trouvilliez, A., Naaim-Bouvet, F., Genthon, C., and Gallée, H.: Present weather-sensor tests for measuring drifting snow, Annals of Glaciology, 52, 176–184, https://doi.org/10.3189/172756411797252356, 2011.

Berne, A. and Uijlenhoet, R.: Path-averaged rainfall estimation using microwave links: Uncertainty due to spatial rainfall variability, Geophysical Research Letters, 34, https://doi.org/https://doi.org/10.1029/2007GL029409, 2007.

Berne, A., ten Heggeler, M., Uijlenhoet, R., Delobbe, L., Dierickx, P., and de Wit, M.: A preliminary investigation of radar rainfall estimation in the Ardennes region and a first hydrological application for the Ourthe catchment, Natural Hazards and Earth System Sciences, 5, 267–274, https://doi.org/10.5194/nhess-5-267-2005, 2005.

Chen, J.-Y., Reinoso-Rondinel, R., Trömel, S., Simmer, C., and Ryzhkov, A.: A Radar-Based Quantitative Precipitation Estimation Algorithm to Overcome the Impact of Vertical Gradients of Warm-Rain Precipitation: The Flood in Western Germany on 14 July 2021, Journal of Hydrometeorology, 24, 521 – 536, https://doi.org/10.1175/JHM-D-22-0111.1, 2023.

Chwala, C. and Kunstmann, H.: Commercial microwave link networks for rainfall observation: Assessment of the current status and future challenges, WIREs Water, 6, e1337, https://doi.org/https://doi.org/10.1002/wat2.1337, e1337 WATER-363.R2, 2019.

Chwala, C., Graf, M., Polz, J., Blettner, N., DanSereb, Øydvin, E., keis, overeem, toufikshit, Kaleta, L., and yboose: pycomlink/pycomlink: v0.5.0, https://doi.org/10.5281/zenodo.17304578, 2025.

Erpicum, M., Fettweis, X., Jorion, N., Pirard, X., Van Campenhout, J., and Sougnez, A.: Laser disdrometer tools for local and climatological characterization of hydrometeors, in: EGU General Assembly Conference Abstracts, EGU General Assembly Conference Abstracts, p. 13940, 2012.

Fencl, M., Bareš, V., Ostrometzky, J., Messer, H., Winterrath, T., Priestley, A., and Chwala, C.: A New Initiative to Facilitate the Global Collection of Microwave Link Data and Its Use in Hydrometeorology, Bulletin of the American Meteorological Society, 106, E438 – E440, https://doi.org/10.1175/BAMS-D-24-0346.1, 2025.

Goudenhoofdt, E. and Delobbe, L.: Evaluation of radar-gauge merging methods for quantitative precipitation estimates, Hydrology and Earth System Sciences, 13, 195–203, https://doi.org/10.5194/hess-13-195-2009, 2009.

Goudenhoofdt, E., Delobbe, L., and Willems, P.: Regional frequency analysis of extreme rainfall in Belgium based on radar estimates, Hydrology and Earth System Sciences, 21, 5385–5399, https://doi.org/10.5194/hess-21-5385-2017, 2017.

Graf, M., Chwala, C., Polz, J., and Kunstmann, H.: Rainfall estimation from a German-wide commercial microwave link network: optimized processing and validation for 1 year of data, Hydrology and Earth System Sciences, 24, 2931–2950, https://doi.org/10.5194/hess-24-2931-2020, 2020.

Graf, M., Wagner, A., Polz, J., Lliso, L., Lahuerta, J. A., Kunstmann, H., and Chwala, C.: Improved rain event detection in commercial microwave link time series via combination with MSG SEVIRI data, Atmospheric Measurement Techniques, 17, 2165–2182, https://doi.org/10.5194/amt-17-2165-2024, 2024.

Graf, M., Bareŝ, V., Messer, H., Nebuloni, R., Fencl, M., Chwala, C., Overeem, A., van de Beek, R., Olsson, J., Ostrometzky, J., Hanna, N., Uijlenhoet, R., Gottschalk, M., and Winterrath, T.: The Opportunistic Precipitation Sensing Network (OpenSense), Bulletin of the American Meteorological Society, pp. BAMS–D–25–0326.1, https://doi.org/10.1175/BAMS-D-25-0326.1, 2025.

https://doi.org/10.5194/egusphere-2026-457
Preprint. Discussion started: 5 March 2026

Hailegeorgis, T. T. and Alfredsen, K.: Analyses of extreme precipitation and runoff events including uncertainties and reliability in design and management of urban water infrastructure, Journal of Hydrology, 544, 290–305, https://doi.org/https://doi.org/10.1016/j.jhydrol.2016.11.037, 2017.

Imhoff, R. O., De Cruz, L., Dewettinck, W., Brauer, C. C., Uijlenhoet, R., van Heeringen, K.-J., Velasco-Forero, C., Nerini, D., Van Ginderachter, M., and Weerts, A. H.: Scale-dependent blending of ensemble rainfall nowcasts and numerical weather prediction in the open-source pysteps library, Quarterly Journal of the Royal Meteorological Society, 149, 1335–1364, https://doi.org/https://doi.org/10.1002/qj.4461, 2023.

ITU: Recommendation ITU-R P.838-3, Specific attenuation model for rain for use in prediction methods, Tech. rep., International Telecommunication Union, https://www.itu.int/dms_pubrec/itu-r/rec/p/R-REC-P.838-3-200503-I!!PDF-E.pdf, 2005.

Johnson, L. E., Cifelli, R., and White, A.: Benefits of an advanced quantitative precipitation information system, Journal of Flood Risk Management, 13, e12 573, https://doi.org/https://doi.org/10.1111/jfr3.12573, 2020.

Journée, M., Goudenhoofdt, E., Vannitsem, S., and Delobbe, L.: Quantitative rainfall analysis of the 2021 mid-July flood event in Belgium, Hydrology and Earth System Sciences, 27, 3169–3189, https://doi.org/10.5194/hess-27-3169-2023, 2023.

Leijnse, H., Uijlenhoet, R., and Stricker, J. N. M.: Rainfall measurement using radio links from cellular communication networks, Water Resources Research, 43, https://doi.org/https://doi.org/10.1029/2006WR005631, 2007.

Leijnse, H., Uijlenhoet, R., and Stricker, J.: Microwave link rainfall estimation: Effects of link length and frequency, temporal sampling, power resolution, and wet antenna attenuation, Advances in Water Resources, 31, 1481–1493, https://doi.org/https://doi.org/10.1016/j.advwatres.2008.03.004, 2008.

Leinonen, J.: High-level interface to T-matrix scattering calculations: architecture, capabilities and limitations, Opt. Express, 22, 1655–1660, https://doi.org/10.1364/OE.22.001655, 2014.

Lengfeld, K., Kirstetter, P.-E., Fowler, H. J., Yu, J., Becker, A., Flamig, Z., and Gourley, J.: Use of radar data for characterizing extreme precipitation at fine scales and short durations, Environmental Research Letters, 15, 085 003, https://doi.org/10.1088/1748-9326/ab98b4, 2020.

Messer, H., Zinevich, A., and Alpert, P.: Environmental Monitoring by Wireless Communication Networks, Science, 312, 713–713, https://doi.org/10.1126/science.1120034, 2006.

Moraux, A., Dewitte, S., Cornelis, B., and Munteanu, A.: A Deep Learning Multimodal Method for Precipitation Estimation, Remote Sensing, 13, https://doi.org/10.3390/rs13163278, 2021.

Nebuloni, R., Cazzaniga, G., D'Amico, M., Deidda, C., and De Michele, C.: Comparison of CML Rainfall Data against Rain Gauges and Disdrometers in a Mountainous Environment, Sensors, 22, https://doi.org/10.3390/s22093218, 2022.

Overeem, A., Leijnse, H., and Uijlenhoet, R.: Measuring urban rainfall using microwave links from commercial cellular communication networks, Water Resources Research, 47, https://doi.org/https://doi.org/10.1029/2010WR010350, 2011.

Overeem, A., Leijnse, H., and Uijlenhoet, R.: Retrieval algorithm for rainfall mapping from microwave links in a cellular communication network, Atmospheric Measurement Techniques, 9, 2425–2444, https://doi.org/10.5194/amt-9-2425-2016, 2016a.

Overeem, A., Leijnse, H., and Uijlenhoet, R.: Two and a half years of country-wide rainfall maps using radio links from commercial cellular telecommunication networks, Water Resources Research, 52, 8039–8065, https://doi.org/https://doi.org/10.1002/2016WR019412, 2016b.

Pastorek, J., Fencl, M., Rieckermann, J., and Bareš, V.: Precipitation Estimates From Commercial Microwave Links: Practical Approaches to Wet-Antenna Correction, IEEE Transactions on Geoscience and Remote Sensing, 60, 1–9, https://doi.org/10.1109/TGRS.2021.3110004, 2022.

https://doi.org/10.5194/egusphere-2026-457
Preprint. Discussion started: 5 March 2026

Prahl, S.: miepython: A Python library for Mie scattering calculations, https://doi.org/10.5281/zenodo.7949263, 2026.

Prudden, R., Adams, S., Kangin, D., Robinson, N., Ravuri, S., Mohamed, S., and Arribas, A.: A review of radar-based nowcasting of precipitation and applicable machine learning techniques, https://arxiv.org/abs/2005.04988, 2020.

Raupach, T. H. and Berne, A.: Correction of raindrop size distributions measured by Parsivel disdrometers, using a two-dimensional video disdrometer as a reference, Atmospheric Measurement Techniques, 8, 343–365, https://doi.org/10.5194/amt-8-343-2015, 2015.

RMI: Legend Rain, https://www.meteo.be/en/weather/warnings/legend-rain, accessed: 2026-01-13.

Roversi, G., Alberoni, P. P., Fornasiero, A., and Porcù, F.: Commercial microwave links as a tool for operational rainfall monitoring in Northern Italy, Atmospheric Measurement Techniques, 13, 5779–5797, https://doi.org/10.5194/amt-13-5779-2020, 2020.

Schleiss, M. and Berne, A.: Identification of Dry and Rainy Periods Using Telecommunication Microwave Links, IEEE Geoscience and Remote Sensing Letters, 7, 611–615, https://doi.org/10.1109/LGRS.2010.2043052, 2010.

Schleiss, M., Rieckermann, J., and Berne, A.: Quantification and Modeling of Wet-Antenna Attenuation for Commercial Microwave Links, IEEE Geoscience and Remote Sensing Letters, 10, 1195–1199, https://doi.org/10.1109/LGRS.2012.2236074, 2013.

Schuurmans, J. M., Bierkens, M. F. P., Pebesma, E. J., and Uijlenhoet, R.: Automatic Prediction of High-Resolution Daily Rainfall Fields for Multiple Extents: The Potential of Operational Radar, Journal of Hydrometeorology, 8, 1204 – 1224, https://doi.org/10.1175/2007JHM792.1, 2007.

Sokol, Z., Szturc, J., Orellana-Alvear, J., Popová, J., Jurczyk, A., and Célleri, R.: The Role of Weather Radar in Rainfall Estimation and Its Application in Meteorological and Hydrological Modelling—A Review, Remote Sensing, 13, https://www.mdpi.com/2072-4292/13/3/351, 2021.

Uijlenhoet, R.: Raindrop size distributions and radar reflectivity–rain rate relationships for radar hydrology, Hydrology and Earth System Sciences, 5, 615–628, https://doi.org/10.5194/hess-5-615-2001, 2001.

Uijlenhoet, R., Overeem, A., and Leijnse, H.: Opportunistic remote sensing of rainfall using microwave links from cellular communication networks, WIREs Water, 5, e1289, https://doi.org/https://doi.org/10.1002/wat2.1289, 2018.

van de Beek, C., Leijnse, H., Torfs, P., and Uijlenhoet, R.: Seasonal semi-variance of Dutch rainfall at hourly to daily scales, Advances in Water Resources, 45, 76–85, https://doi.org/https://doi.org/10.1016/j.advwatres.2012.03.023, space-Time Precipitation from Urban Scale to Global Change, 2012.

van het Schip, T. I., Overeem, A., Leijnse, H., Uijlenhoet, R., Meirink, J. F., and van Delden, A. J.: Rainfall measurement using cell phone links: classification of wet and dry periods using geostationary satellites, Hydrological Sciences Journal, 62, 1343–1353, https://doi.org/10.1080/02626667.2017.1329588, 2017.

van Leth, T. C., Overeem, A., Leijnse, H., and Uijlenhoet, R.: A measurement campaign to assess sources of error in microwave link rainfall estimation, Atmospheric Measurement Techniques, 11, 4645–4669, https://doi.org/10.5194/amt-11-4645-2018, 2018.

Van Weverberg, K., Ghilain, N., Goudenhoofdt, E., Barbier, M., Koistinen, E., Doutreloup, S., Van Schaeybroeck, B., Frankl, A., and Field, P.: Sensitivity of simulated rain intensity and kinetic energy to aerosols and warm-rain microphysics during the extreme event of July 2021 in Belgium, Quarterly Journal of the Royal Meteorological Society, 150, 3322–3345, https://doi.org/https://doi.org/10.1002/qj.4761, 2024.